Anonymous Referee #1

First of all. A heartfelt thank you for the thorough review of the paper. We very much appreciate the time and effort reviewer 1 put into the review, and we believe that he or she enabled a considerable improvement of the article, especially with regard to the choice of our a priori error covariance. In the following we address the reviewer's comments in detail. All changes are highlighted in a track changes version of the manuscript.

Initial Review

1. there are many grammar mistakes. These should be corrected before accepting the manuscript.

We have given the manuscript to a native English speaker to correct the mistakes and included his corrections.

2. Some conclusions reported in the abstract are not supported by the results. Such as for frozen hydrometers "Profile retrievals may be possible for the mass densities and some information about the microphysical properties, especially for cloud ice, can be gained." and for liquid hydrometer "There is little information about the profile or the microphysical properties".

We have thoroughly revised the definition of the a priori error covariance, which changed the results (see below). We adjusted the abstract accordingly.

Review of manuscript: 'All-sky Information Content Analysis for Novel Passive Microwave Instruments in the Range from 23.8 GHz up to 874.4 GHz' by V. Grützun et al.

General

This paper attempts to address issues related to the information content of space-borne microwave and sub-millimeter observations of clouds and precipitation. In particular it uses linear optimal estimation theory to quantify the information content of novel spaceborne sensors that currently are being developed (ICI) and of existing airborne sensors (ISMAR and MARSS). This is an interesting, timely, and relevant topic. However, unfortunately, this paper has a couple of fundamental flaws and shortcomings and I cannot recommend publication at this point. Beyond this, I am also somewhat skeptical of the relevance and global applicability of the results presented, even if the flaws were corrected. My major criticisms are as follows.

1. Major comments
1.1. The calculation of the a-priori covariance matrix Sa is flawed

Calculating Sa in log-space for positive semi-definite quantities such as SWC poses the challenge of what to do with the zeros, as correctly stated by the authors. However, their approach of setting zeros to 2.22E-16 to numerically avoid this issue will have a significant impact on Sa and DOF.

A simple example: Assume a quantity (e.g. SWC) for which we have two-hundred values (e.g. SWC at 500 hPa from 200 profiles). Say, one-hundred of these values are zeros ('cloud-free') and one-hundred are 0.1 (in some appropriate units). What is the variance of log(SWC) now? If I set the zeros to 2.22E-16, take the logarithm of this two-hundred element vector, and calculate its variance, the variance comes out to be ~286. But why chose 2.22E-16, would not a good approximation for zero be 1E-10? If I do that, the variance is reduced to ~107. If I assume 1E-8 is zero, then the variance becomes ~65. Or, maybe I should assume double-precision? In that case I can set the zero SWC values to, say, 1D-50 and the variance becomes ~3200. Whichever number it is, this number will populate the diagonal elements of Sa. So, ultimately Sa becomes arbitrary.

This issue is only slightly ameliorated if there are fewer 'cloud-free' observations that have to be replaced because whichever small number I chose to fill in the zeros, they will constitute outliers and dominate the variance and thereby Sa. This also explains the authors statement that 'The covariance […] goes up to 670 in units of the natural logarithm on the diagonal of the SWC-SWC block matrix'.

This will have tremendous effects on the value of DOF. The larger Sa becomes, the larger DOF will be. That is, the less the a-priori is constrained, the more influence the measurements will have. Below is an example of this using a very simple fictional observing system with two observations and two elements of the state space (and identity Jacobians, which have no impact on the principal point made here.)

Again, the point is: The magnitude of Sa relative to Sy will have a very strong impact on DOF. The larger the values of Sa, the higher DOF will be. If the choice of Sa is arbitrary, the resulting DOF will be arbitrary. This issue in itself invalidates the paper results.

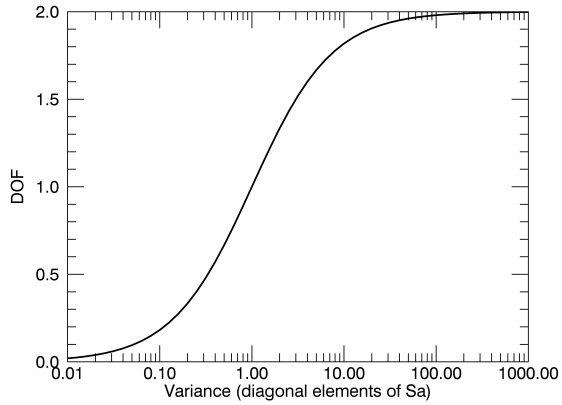

Figure 1 Plot shows the strong dependence of DOF on the magnitude of Sa relative to Sy.

We are very grateful for this comment, and for the effort you have put into this point! We agree with your arguments and have re-evaluated the definition of our a priori covariance (see entire Section 4.2 "A priori covariance"). In fact, the new definition gives far more physical results for the information content. Especially, we now get some ability to detect liquid clouds and rain better (Fig. 10 and 12, Tab. 4), which, on a second thought, makes much

more sense, because our set of channels includes five channels in the 118 GHz region, and one at 89, 50, and 23 GHz each. These channels are indeed sensitive to liquid hydrometeors. Also, as you pointed out, Bauer and Mugnai showed that an extended (compared to the instruments we use) set of channels around the 118 GHz oxygen line and within the oxygen absorption complex region between 50 and 57 GHz gives good results for profile retrievals of precipitation. We do not expect equally good results in our case, because we would need more lines within the absorption complex around 50 GHz, but we indeed should have paid more attention to the fact that the information content for liquid cloud and rain was so low.

We are aware that the choices we make for our a priori matrix will have an influence on the variance and therefore on the information content. This is the case in each optimal estimation retrieval, and finding a suitable a priori covariance is one of the challenges in doing such retrievals. For the revised version of the article, we have employed more reasonable and justifiable thresholds as follows, and we also discuss the influence of the choices in more detail in the result section (see below).

1. We assume that we have a working algorithm to detect clouds in the first place and only include cloudy columns. The criterion for "cloudy" for the profiles of the ICON simulation is that the total condensed water path exceeds 1e-4 kg m^{-2}. This threshold, however, does not affect the results much. Furthermore, we include all available time steps of the simulation, such that the number of profiles for the calculation is increased (we chose the cloudiest time step in the initial article draft).

2. We now clip the values instead of only setting the zeros to our thresholds. Clipping in our sense means that any value, which is smaller than the threshold value is set to the respective threshold. With the very small numerical threshold, this did not make much of an effect, but with the larger thresholds (see below), this has a great influence on the variance of the system.

3. For the mass densities, we employed a threshold of 1e-7 kg m^{-3}. Assuming a detection limit for, e.g., cloud ice water path of 1 g m^{-2} (see e.g. Brath et al., 2018), and a cloud thickness of about 2.5 km, we end up with a cloud ice mass density threshold in the order of 1e-7 kg m^{-3}. This also approximately corresponds to a numerical threshold within the two-moment scheme (approximately, because the scheme employs mass mixing ratios instead of mass densities). Beyond this value, for example collisional processes can take place.

4. For the mean particle masses, we employed the intrinsic lower thresholds of the two-moment scheme. We have experimented with setting the threshold in dependence of the threshold for the mass densities, but this introduced artificial correlations between the two quantities which were not present in the first place.

With the chosen thresholds, the main peaks of the distribution of the hydrometeor mass densities (and by definition also of the mean masses) are considered for the calculation of the a priori covariance. These main peaks are the physically meaningful values within the simulation and therefore should be, and with the chosen thresholds are, included in the calculation.

The threshold for the mass densities has the biggest influence. We have explored the dependency of the mean information content on this particular threshold (see Figure 2, which is also included in the revised manuscript as Fig. 11). The principle relations between the information content for the mass densities stay the same, but naturally the overall information content decreases for an increasing threshold. The information content for the mean masses on the other hand somewhat increases. This is based on the combined retrieval and influenced by the cross correlations between the mass densities and the mean masses, since the threshold for the mean masses stays constant over the whole plot. The chosen threshold of 1e-7 for the mass density gives reasonable results for the information content.

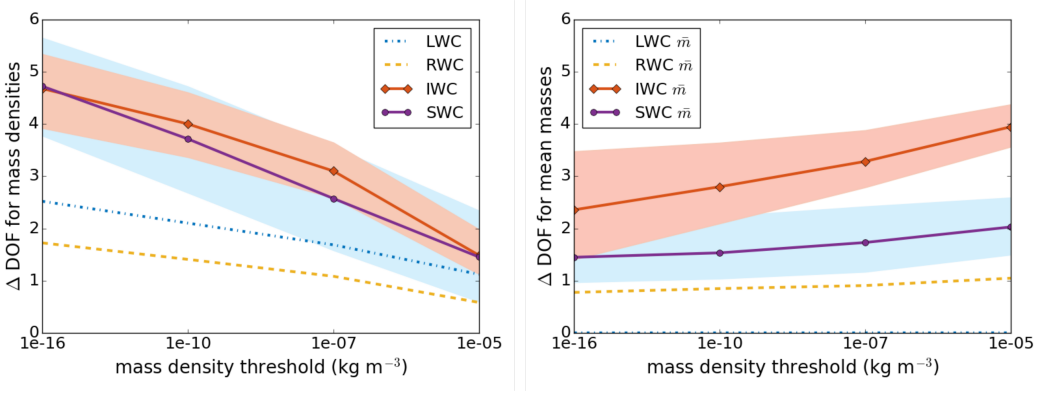

Figure 2 Information content, dependence on chosen threshold. Left: ΔDOF for mass densities. Right: ΔDOF for mean masses. The threshold for the mass densities is altered, the one for the mean masses stays constant. The line shows the mean information content, the shaded area lies between the minimum and maximum information content. The dependency of the information content of the mean masses on the threshold for the mass densities is due to the covariance or the respective cross correlations of mass densities and mean masses.

The new a priori covariance matrix first is more consistent with the microphysical scheme on the one hand, second has more physical based thresholds to clip small values from the profiles, and third also gives more reasonable results for the information content. We have included some discussion about the dependencies in the manuscript (mainly p24, l5 – p25, l6 and Fig. 11). We think that we found a much better definition than in the initially submitted manuscript which satisfies the requirements of the information content analysis much better. Thank you again for your this very valuable comment, which made us think much more thoroughly about the applied assumptions for the a priori error covariance!

1.2. Too small variability in underlying dataset

This study is based on a very limited set of model data (one mid-latitude frontal event). While the sensitivity study regarding the one average profile and the 90 selected profiles does show some variability, tropical, mid-latitude wintertime and other situations are simply not captured by this study. These situations will not only likely have dramatically different a-priori covariance, but also dramatically different Jacobians. For example, in a very dry atmosphere, the sounding capabilities at higher frequencies will be reduced as more and more channels might see further down in the atmosphere. This will decrease DOF. Similarly, in a very intense

tropical deep convective area, nearly all weighting functions that peak in the mid- and lower troposphere will move up because the atmosphere becomes optically very thick. This, again, will increase redundancy and reduce DOF. While the authors acknowledge the shortcomings of the limited dataset, none of these effects is quantified or even discussed.

So, even if the methodology was right and Sa was calculated correctly, the results will be of very limited use in characterizing the instruments.

Yes, the use of one case limits the study to some extent. We believe that the basic principles can be made clear on the basis of this case, especially the interdependencies of the Jacobians. We acknowledge that the Jacobians will look different in different regimes and have added some phrases regarding this topic to the discussion (p4, l10-14).

1.3. Key concept for lower frequencies missing

A key novel concept of the Metop-SG constellation is the combination of the 118 GHz and 50-60 GHz oxygen sounding channels for precipitation retrievals as outlined for example in Bauer and Mugnai (2003)[1]. This aspect is completely ignored in the current study and only a reduced set of three channels below 118GHz is even considered, none of which are sounding channels. Therefore, the authors conclusion that 'The information about the liquid hydrometeors comes from the lower channels and is comparably low (2.36 for liquid cloud water and 1.81 for rain).' appears to not be justified. A fair assessment of this statement with regard to Metop-SG would have to include the full set of MWI channels sounding channels. For the case of the airborne MARSS system, the finding is probably correct, but given there are only three low-frequency channels it is no surprise the information content comes out to be somewhere between one and three. This is also consistent with the existing large body of literature on lowfrequency precipitation and cloud liquid water retrievals.

I suggest either this is addressed in full (including the 50-60 sounding channels), or at the very least much more emphasis is put on this aspect and/or the very limited nature of this particular finding be highlighted.

The focus of our study was more on the instruments ICI and ISMAR, complemented by a few lower frequency channels from the instrumentation which has been flown on the FAAM aircraft. We did not intend to put our focus on the full microwave suite of Metop-SG. We should have stated that clearer in the initial manuscript, and apologize for the oversight! We now have put more emphasis on the fact that we do not expect to gain a large amount of information about liquid hydrometeors with the channels, which we employ (e.g. p22, l3 – 9, again stressed in conclusions p28, l15-17). We have emphasized that our focus is more on the detection of frozen hydrometeors with the instruments ICI and ISMAR. However, with the newly defined a priori error covariance, liquid water gains a greater proportion of the total information content, which stems from the 23, 89, 50 and the outer 118 GHz lines (Fig. 10, Tab. 4). It seems that the initially defined a priori error favoured frozen hydrometeors more than liquid ones. We changed our discussion accordingly and more thoroughly included the fact that more channels in the lower frequency regions are needed to retrieve liquid hydrometeor retrievals and we stressed that precipitation retrievals with these low channels are established techniques (as above, p22, l3 - 9). We have included the information that such

low frequency channels will be available on the Metop-SG satellite (p27, l14 - 17). We also have included the reference Bauer and Mugani, 2003.

[1] Bauer and Mugnai: JGR, VOL. 108, NO. D23, 4730, doi:10.1029/2003JD003572, 2003

2. Other comments

Page 5, Line 19/20: "It is crucial to match the microphysical parameterisations of the radiative transfer model with those of the atmospheric model." I do not agree with this. It would be perfectly fine to use for example different habits that are not consistent with the assumptions made in the ICON microphysics parameterizations, e.g. in the m-D relationship. The variability imposed by ice habits on the simulations (and thereby also on Sy) is not discussed.

Thank you for pointing this out. You are right, the m-D relationship in the microphysical model is only implicitly used, e.g. for the calculation of fall speeds. Therefore, an inconsistency with regard to this parameter would probably be less crucial than an inconsistency in the employed size distributions. We still would like to use as much information from the two-moment scheme as possible to perform our analysis. We have included some discussion about this in lines (p6, l22 – p.7, l3).

Forward model errors are not accounted for in general in Sy, which only seems to account for reasonable estimates for instrument noise (1 K).

This is true. Within the scope of this study, we assume we have a perfect forward operator. We have added the information in line (p8, l29 – p9, l2).

Page 10, line 8-9: "Instead, the scattering solver for the perturbations gets the reference result as a first guess, which saves most of the iterations that would otherwise be needed." Why first guess? I do not understand. Needs more explanation.

For clarity, we have rephrased this explanation as follows:
"In practice, we do not make a fully independent T_B calculation for each perturbation, since this is computationally very inefficient for the iterative scattering solver used (Emde et al., 2004). Instead, the scattering solver uses the result from the unperturbed scheme as a starting point. That result should be close to the result from the perturbed case already, because our profile perturbations are small. From that starting point, the perturbed Jacobians are calculated with far fewer iterations compared to a completely uneducated starting point, which makes the scheme far more computationally efficient." (p10, l11-16)

E. g. Figure 11: Use of term "LWC Path" etc is confusing… Should be LWP ('Liquid Water Path'). In general the distinction between 'content' and 'path' is somewhat blurry in the paper. The authors jump between the two but consistently use e.g. LWC.

We have included the term "LWP", "IWP", … for the liquid water path, ice water path, … (p5, l19-20) and use it more consistently throughout the article, including a corrected Figure 11.

The impact of what the authors call ‘shielding’ is much better understood in terms of path integrated properties. For example, for ‘shielding’ it matters how much ice in total (in kg/m2) is above the liquid, whereas IWC (in kg/m3) is only of secondary importance. This should be made clearer and the discussion should be expanded.

We have expanded the discussion (line mainly p16, l8-15). We acknowledge the fact that the paths in combination with the sensitivity of the respective channels in the regions where hydrometeors reside are the main contributors to the signal at the top of the atmosphere. Also, we agree that the term “shielding” implies that a hydrometeor below a region with high H2O or a large path of another hydrometeor such as cloud ice, is hidden. We introduced the term to imply that H2O or another hydrometeor between the one to be detected and the sensor is not seen because the sensor can’t penetrate the atmosphere down to the hydrometeor to be detected. We now use the term “shielding” more sparsely and swapped it for “weakening” where applicable.

Part of the weakening of the signal is also due to the specific radiative background, which the other hydrometeors and H2O create. Depending on the radiative background, the signal also might strengthen. For example, in Figure 7 it is evident that the Jacobians for H2O change much in exactly those regions where the cloud ice is located and the cloud ice Jacobians peak. This implies that it is not only the atmospheric part above the regarded component, which alters the signal from that component.

Page 14, near Figure 3 or Table 3: Please provide column integrated values of LWP, IWP, SWP, and H2O and RWP….. This would be very helpful in getting a feeling for the atmosphere.

We have provided the values in the figure caption of Figure 3.

(Page 25, Lines 17) to (Page 26, line 3) are largely just a repetition of the introduction and other parts of Section 2. Should be removed.

We have considerably shortened the paragraph. We would like to keep at least a small introduction in the conclusions and hope that the shortened version is acceptable.

Page 26, Line 6: ‘…its presence shields or strengthens….’ Instead of ‘shields vs strengthens maybe use increases/decreases or weakens/strengthens (something ‘shielding’ something else could, I presume, by used as the explanation for why a weakening occurs in this context.

We have changed to “weakens/strengthens”.

3. Minor comments

Page 3, Line 34: in Sec. 2..

We have corrected this.

Page5, line 4 I suggest ‘are somewhat smaller…’

We didn’t find a phrase matching this comment in that line on p. 5. Did you mean p. 7 l. 4 “the largest snow hydrometeors are little bit smaller smaller than in the two-moment scheme”? We have completely altered that section and the respective phrase doesn’t exist anymore.

Page 25, Line rephrase ‘whole bunch’ with ‘sum of the two’ or something similar.
We have rephrased to: “we gain information about the whole set of frozen hydrometeors”.

Interactive comment on "All-sky Information Content Analysis for Novel Passive Microwave Instruments in the Range from 23.8 GHz up to 874.4 GHz" by Verena Grützun et al.

Anonymous Referee #2
Received and published: 5 January 2018

We thank Referee #2 for his or her time and effort, and for the very valuable comments. We have clarified and corrected the manuscript accordingly (the individual comments are addressed below). Note that due to some major comments of Referee #1 there were major changes in the manuscript. Especially, Referee #1 critisised the choices we made for the calculation of the a priori covariance error from ICON. We therefore recalculated it with more consistent and physically based assumptions. This changes the results for the information content. The general conclusions remain valid, but the liquid phase gains a greater share of the overall information content.

This is a comprehensive study on the idealized information content from microwave/sub-millimeter microwave channels that are relevant to the current instruments deployed in field and space missions.

I have three major comments:

1. I agree with the author that it is highly important to have consistent micro-physical parameterisations in the RTM and atmospheric model and appreciate the careful discussions on the comparisons between Seifer and Beheng 2006 and McFarquhar and Heymsfield (1997) schemes. However, the McFarquhar and Heymsfield (1997) parameterization is developed for tropical cirrus cloud using field campaign data collected during CEPEX, which may not be proper to apply to a midlatitude frontal cloud system. Besides, I don't see why it is necessary to have such long discussions in this article if two-moment scheme is used in both ICON and ARTS.

Thank you for this very valuable suggestion. We have reorganized the discussion of the microphysics. We have much more focused on the two-moment physics and removed the major part of the discussion of the McFarquhar and Heymsfield scheme, including the respective figure. We left a paragraph in, which points to the difference between the two schemes, but we added the information that the one-moment scheme is developed for the tropics (Sec. 3.1, esp. p6, l15-21).

2. In the calculation of Jacobians, the channel response function is not used and instead monochromatic radiative transfer simulations for the center frequencies of the side bands are carried out. For channels in the window region and sounding channels far from the absorption line center, the sensitivities or information content are sensitive to the width of the channel. And these channels are used to retrieve the hydrometeors.

We have added the following to the discussion:

"We do not use an explicit sensor response function but perform monochromatic radiative transfer simulations for the center frequencies of the side bands in each channel and use the mean of the two brightness temperatures. For clear sky, highly resolved (in terms of frequencies) tests showed that the error compared to using one monochromatic frequency per side band is less than 1 K (Brath et al., 2018). Because the scattering properties of the hydrometeors change only marginally within the band width, a further increase of this uncertainty in the cloudy case is unlikely."

Brath, M., Fox, S., Eriksson, P., Harlow, R. C., Burgdorf, M., and Buehler, S. A.: Retrieval of an IceWater Path over the Ocean from ISMAR and MARSS millimeter/submillimeter brightness temperatures, Atmos. Meas. Tech. Discuss., doi:10.5194/amt-2017-167, 2018.

3. P10. Line 8: please explain in more detail: "the scattering solver for the perturbations gets the reference result as a first guess". Scattering is important since the focus of this study is to understand the information content in these channels to the different combination and types of hydrometers.

For clarity, we have rephrased this explanation as follows:
"In practice, we do not make a fully independent T_B calculation for each perturbation, since this is computationally very inefficient for the iterative scattering solver used (Emde et al., 2004). Instead, the scattering solver uses the result from the unperturbed scheme as a starting point. That result should be close to the result from the perturbed case already, because our profile perturbations are small. From that starting point, the perturbed Jacobians are calculated with far fewer iterations compared to a completely uneducated starting point, which makes the scheme far more computationally efficient." (p10, l11-16)

Minor comments:

1. In the abstract, Line 14: "however the information content is robust", this is right after the discussion on the little information on the profiles and microphysics. "robust" with respect to what?
We have rephrased to: "…the information content is surprisingly robust across different atmospheric compositions."

2. P2, Line 34: suggests to change to "low level clouds have only little effect on the "
We have rephrased to: "Low level clouds have only a marginal effect on…"

3. P3. Line 25: remove comma in 183GHz.
We have corrected this.

4. P3. Line 34: add "in" before "Sect.2".
We have corrected this and rephrased slightly.

5. P4. Line 24: Suggest to remove the first sentence in this paragraph, and state what kind of assumptions are made for surface emissivity and surface type.
We have rephrased the paragraph to:

"The radiative transfer simulations were performed with two different surface emissivities ε. In the first set of simulations, ε is equal to 0.6, which corresponds to an ocean surface. In the second set of simulations, ε is equal to 0.9, which corresponds to a land surface. Further, specular reflection is assumed. One should keep in mind though, that in reality ε depends strongly on the specific surface and to a smaller extent on the channel. However, the results differ only little for the different emissivities. Therefore, we use the simplified assumption of a constant emissivity for all channels, and the main part of the results shown in this article will be for the emissivity of the ocean, i.e., ε=0.6." (p5, l3-8)

6. P7, Line 4: "smaller smaller"
The respective section has changed much, and this phrase does not exist anymore.

7. P12, Line 19: "to choose them". Also, should it be "for each hydrometeor type"?
We have corrected both and slightly rephrased (now p13, l18-19).

Line 18: "amongst the extremes": does this mean extreme profiles are selected? If so, it is contradict with following statement that outliers are excluded. Please clarify.
We have rephrased to:
"To exclude unphysical outliers, which may be produced by the model, we disregard the profiles with a path larger than the 99th percentile." (p13, l19-20) Occasionally unphysical values may appear due to numerical issues. In order to only include valid profiles, we exclude the upper percentage of the extreme profiles.

8. P24, Line 8: "has to be paid"
We have corrected this (now p26, l11).

All-sky Information Content Analysis for Novel Passive Microwave Instruments in the Range from 23.8 GHz up to 874.4 GHz

Verena Grützun[1], Stefan A. Buehler[1], Lukas Kluft[2], Jana Mendrok[3], Manfred Brath[1], and Patrick Eriksson[3]

[1]Meteorologisches Institut, Fachbereich Geowissenschaften, Centrum für Erdsystem- und Nachhaltigkeitsforschung (CEN), Universität Hamburg, Bundesstraße 55, 20146 Hamburg, Germany
[2]Max-Planck-Institut für Meteorologie, Hamburg, Germany
[3]Department of Space, Earth and Environment, Chalmers University of Technology, 41296 Gothenburg, Sweden

Correspondence to: Verena Grützun (verena.gruetzun@uni-hamburg.de)

Abstract.

We perform an all-sky information content analysis for channels in the millimeter/submillimeter wavelength with 24 channels in the region from 23.8 up to 874.4 GHz. ~~Our~~ The employed set of channels corresponds to the instruments ISMAR and MARSS, which are available on the British FAAM research aircraft, and it is complemented by two precipitation channels at low frequencies from Deimos. The channels also cover ICI, which will be part of the MetOp-SG mission. We use simulated atmospheres from the ICON model as basis for the study and quantify the information content with the reduction of degrees of freedom (ΔDOF). The required Jacobians are calculated with the radiative transfer model ARTS. Specifically we focus on the dependence of the information content on the atmospheric composition. In general we find a high information content for the frozen hydrometeors, which mainly comes from the higher frequency channels beyond 183.31 GHz (on average ~~4.99~~ 3.10 for cloud ice and ~~4.84~~ 2.57 for snow). ~~Profile retrievals may be possible for the mass densities and some~~ Considerable information about the microphysical properties, especially for cloud ice, can be gained. The information about the liquid hydrometeors comes from the lower ~~channels and is comparably low (2.36~~ frequency channels. It is 1.69 for liquid cloud water and ~~1.81 for rain). There is little information about the profile or the microphysical properties~~1.08 for rain using the full set of channels. The Jacobians for a specific cloud hydrometeor strongly depend on the atmospheric composition. Especially for the liquid hydrometeors ~~they~~ the Jacobians even change sign in some cases. However, the information content is robust across different atmospheric compositions. For liquid hydrometeors ~~it slightly~~ the information content decreases in the presence of any frozen hydrometeor, for the frozen hydrometeors it ~~slightly decreases~~ decreases slightly in the presence of the respective other frozen hydrometeor. ~~The~~ Due to the lack of channels below 183 GHz liquid hydrometeors are hardly seen by ICI. But the overall results with regard to the frozen hydrometeors ~~in principle~~ also hold for the ICI sensor. This points to ~~its~~ ICI's great ability to observe ice clouds from space on a global scale with a good spatial coverage in unprecedented detail.

1 Introduction

In the last years, passive millimeter/sub-millimeter wavelength measurements of the cloudy sky from space have gained increasing attention. Especially frozen clouds are in the focus of such measurements. ~~And this with a good reason , because clouds are important factors~~ The reason being that clouds are an important factor in the climate system. For decades ~~they~~ clouds have contributed to the largest uncertainties to estimating the Earth's changing energy budget (Boucher et al., 2013). Also, the assimilation of the cloudy sky in numerical weather forecasting ~~becomes increasingly important (Guerbette et al., 2016)~~is becoming increasingly important (Guerbette et al., 2016; Geer et al., 2017). To constrain the estimation of the future development of the climate system and to assimilate the cloudy sky into the weather forecast, reliable global observations of clouds are required. Passive millimeter/sub-millimeter wavelength measurements have a great potential to fill that gap.

Many studies have investigated the performance of setups, which employ channels in the range from 5 ~~GHz~~ up to 874 GHz. For example, Di Michele and Bauer (2006) focus on channels between 5 and 200 GHz. They find different suitable frequency bands for rain over ocean, snow over land and ocean, and clouds over ocean and suggest several channels covering these frequency ranges for global and multi-seasonal applications. Jiménez et al. (2007) investigated an instrument with twelve channels around the 183, 325 and 448 GHz water vapour lines and the 234, 664 and 874 GHz window channels. A five-receiver instrument dropping one of the two highest channels proved to be equally powerful in a mid-latitude scenario as the all-receiver instrument, but for tropical scenarios the highest channel reduced the error for very thin and high clouds. Also, new studies investigate the potential to assimilate microwave sounding data from geostationary satellites into numerical forecast models to further improve ~~the forecast~~ these models (Duruisseau et al., 2017).

There are already very successful ~~missions ongoing~~ ongoing missions, which, amongst other things, observe clouds from space. A well-known instrument, which ~~is~~ has been observing the atmosphere from space for decades now, is the Advanced Microwave Sounding Unit B (AMSU-B, Weng et al. (2003); Zhao and Weng (2002)) and its successor, the Microwave Humidity Sounder (MHS, Bonsignori (2007)). AMSU-B ~~operates with five channels in the range from 89 GHz to 183.31 GHz and MHS~~ and MHS operate with five channels in the range from 89 ~~GHz~~ up to 190 GHz, respectively. Although the instruments are primarily designed as humidity sounders, as a side product they also allow for an observation of the ice water path (column integrated ice water mass), rain rate and snow water equivalent.

In the near future, the Meteorological Operational Satellite - Second Generation (MetOp-SG, Pica et al. (2012)) with the new Ice Cloud Imager (ICI) will be launched. The principle of ICI is explained in the CloudIce mission proposal for ESA's Earth Explorer 8 ~~(Buehler et al., 2012, 2007)~~(Buehler et al., 2007, 2012). ICI has in total 11 channels in the range from 183.31 ~~GHz~~ to 664.0 GHz and will provide several ice retrievals including the ice water path and the cloud ice effective radius. It will be flown together with the MicroWave Imager (MWI), which has 18 channels in the range from 18.7 ~~GHz~~ up to 183.31 GHz (see e.g. Accadia et al., 2013, for detailed information about ICI and MWI). The inclusion of the low channels in these instruments allows for precipitation retrievals.

In recent years, ~~also~~ the potential of hyper-spectral sensors in the millimeter/submillimeter wavelength region ~~is~~ has been explored for clear-sky (~~Mahfouf et al. (2015)~~Aires et al. (2015); Mahfouf et al. (2015)) and cloudy-sky (~~Birman et al. (2017)~~Birman et al. (20

conditions. Birman et al. (2017) find that the information content on hydrometeors can be significantly increased by using a hyper-spectral sensor, but also depends on the assumed microphysical properties of the frozen hydrometeors.

The different hydrometeor types have different effects on the measurement channels. Several studies focused on the influence of clouds and precipitation on AMSU-like channels around 89, 150 and 183.31 GHz (e.g. Hong et al., 2005; Sreerekha et al., 2008, and references therein). It was found that high level clouds with high cloud tops cause a brightness temperature depression in the channels with frequencies greater than 150 GHz~~, and that low level clouds only little affect~~. Low level clouds have only a marginal effect on the 183.31 GHz channel because the largest sensitivity of that channel is too high up in the atmosphere (Burns et al., 1997; Bennartz and Bauer, 2003). For the same reason, the surface emissivity does not contribute to the signal in these channels. The channel at 89 GHz on the other hand is influenced by altostratus liquid clouds (Muller et al., 1994). Furthermore it is very sensitive to the surface emissivity. Even though the channel at 150 GHz is also a window channel, it shows much less sensitivity to the surface because the region with highest sensitivity to changes in the atmospheric column is located in the lower troposphere above the surface (Bennartz and Bauer, 2003; Hong et al., 2005). Also the Megha-Tropiques mission (*megha* is the Sanskrit word for clouds, tropiques the French word for tropics, Desbois et al., 2002; Karouche et al., 2012) allows an ice cloud content profile retrieval from the Microwave Analysis and Detection of Rain and Atmospheric Systems (MADRAS sensor, Defer et al. (e.g. 2014)) with channels at 89 ~~GHz~~ and 157 GHz.

Greenwald and Christopher (2002) found that precipitating cold clouds give a much stronger signal in channels near 183.31 GHz compared to cold clouds which are not precipitating. They question the applicability of channels near or below 183.31 GHz to gain quantitative estimates of physical properties of non-precipitating ice clouds from space.

In fact, it is very likely that the presence of one hydrometeor type affects the observation of another in the passive observation in the millimeter/sub-millimeter range~~, because~~. The reason is that the signal, which is observed at the top of the atmosphere by the satellite is a result of the interaction of the radiation with each atmospheric component present in the pathway. In this article, we specifically focus on this effect in detail. In the following, we study the information content of passive microwave measurements of clouds from space with specific focus on the cloudy atmosphere, especially on frozen hydrometeors. We investigate whether it depends on the combinations of cloud and precipitation hydrometeors within the atmospheric column how much information ~~we get~~is obtained, as the results from Greenwald and Christopher (2002) suggest. To include higher channels, which may be suitable to detect ice microphysical properties, we chose the setup of the instruments MARSS (Microwave Airborne Radiometer Scanning System, McGrath and Hewison (2001)) and ISMAR (International Sub-millimeter Microwave Airborne Radiometer, Fox et al. (2017)) and complement them by two low channels at 23.8 ~~GHz~~ and 50.1 GHz from Deimos (Dual-frequency Extension to In-flight Microwave Observing System, Hewison (1995)). These instruments cover a large range of microwave channels from 23.8 ~~GHz~~ up to 874.4 GHz (see Sect. 5.1), including the ICI channels, and part of MWI. Thus we can put ~~our~~ the focus on the potential of novel instruments operating at frequencies higher than 183 GHz to robustly observe ice, but also include liquid clouds and precipitation, which ~~is~~ are observed with the channels lower than 183~~,~~ GHz.

Since it is impossible to have full knowledge of the real atmosphere, we chose to base our investigations on high-resolution model data from the ICOsahedral Non-hydrostatic model (ICON model, Dipankar et al. (2015); Heinze et al. (2017)), which employs the two-moment microphysics by Seifert and Beheng (2006). We use the reduction of degrees of freedom as a tool to

quantify the information content of a measurement with regard to a certain hydrometeor. For this purpose we require Jacobians, which we explicitly calculate with the Atmospheric Radiative Transfer Simulator (ARTS, ~~Buehler et al. (2005); Eriksson et al. (2011))~~Bueh
We first use an idealised mean profile to ~~do~~ perform a conceptual study of the mechanisms and then look into a larger set of atmospheric profiles from ICON with the full set of channels and with the channel set corresponding to ICI to investigate if the results hold for more realistic atmospheres.

In the following, ~~we first introduce~~ first the underlying modeling framework is introduced in Sect. 2. Secondly, ~~we present in detail~~ the microphysical assumptions for the atmospheric and for the radiative transfer model, which we use in ~~our study,~~ this study, are introduced in Sect. 3. ~~Our~~ The framework to quantify the information content is presented in Sect. 4. We explain the choice of an idealised atmospheric profile and of 90 realistic profiles, as well as the selected set of channels in Sect. 5. ~~Our~~ The results are presented in Sect. 6. Finally we conclude the article in Sect. 7.

2 Models

2.1 ICON

~~We base our study~~ This study bases on data from the novel ICOsahedral Non-hydrostatic model (ICON model, e.g. Wan et al., 2013; Dipankar et al., 2015). We use a simulation of a frontal case on 26 April 2013 over ~~West~~ western Germany with rapidly increasing cloudiness to a completely overcast situation in the afternoon. Several light to medium rain showers ~~happened~~ occured during that day, and ice clouds as well as snow in the upper atmospheric layers were ~~found. The~~ observed. The case represents a spring day in the northern mid-latitudes. Choosing a tropical case or a much drier case, for example in the arctic, will have an effect on both the Jacobians and the resulting information content. The Jacobians will peak at different heights, and the channels will observe the hydrometeor content depending on how far down they penetrate the atmosphere. Nevertheless, the principles of the observation and the interdependencies of the Jacobians can be made clear at the hand of this case.

The ICON simulation has a horizontal resolution of 650 m with 50 hybrid terrain-following vertical height levels up to 22 km. It was performed in the framework of the BMBF project High Definition Clouds and Precipitation for advancing Climate Prediction (HD(CP)^2) and was provided by the Max-Planck Institute for Meteorology, Hamburg. The simulation complements the measurement campaign HOPE (HD(CP)^2 Observation Prototype Experiment, Macke et al. (2017a)) which took place in April and May 2013 around Jülich in the West of Germany and focused on clouds and model evaluation (e.g. Stamnas et al., 2016; Heinze et al., 2017; Macke et al., 2017b)[1].

[1]Details about the project and the campaign can be found on the project homepage http://hdcp2.eu (last assessed July 2017) or on the data base SAMD (Standardised Atmospheric Measurement Data) homepage hosted at the Integrated Climate Data Center (ICDC) under http://icdc.cen.uni-hamburg.de/1/projekte/samd.html (last assessed ~~July 2017~~April 2018). A special issue of Atmospheric Chemistry and Physics (ACP) about HOPE has been issued (HD(CP)2 Observational Prototype Experiment (AMT/ACP inter-journal SI), 2014, Eds. S. Buehler and H. Russchenberg).

2.2 Atmospheric Radiative Transfer Simulator ARTS

In order to perform an information content analysis a radiative transfer model is required to simulate the satellite measurements and the respective height-resolved Jacobians based on the atmospheric profiles simulated by ICON. We use the Atmospheric Radiative Transfer Simulator ~~(ARTS, Buehler et al., 2005; Eriksson et al., 2011, version 2.3.296)~~(ARTS, Buehler et al., 2005, 2018; Erik
ARTS is an open source detailed line-by-line radiative transfer model for microwave to thermal infrared radiation, which is capable ~~to simulate~~ of simulating polarised radiative transfer in all spatial geometries[2]. ARTS offers analytical Jacobians for trace gas concentration, and semi-analytical Jacobians for temperature. In this ARTS version, Jacobians for hydrometeor parameters are calculated by perturbation, which has higher computational costs compared to analytical computation. Details about the calculation of these Jacobians are given in Sect. 4.1~~and the~~. The specific setup of ARTS is described in Sect. 3.2.

~~For the radiative transfer calculations we have to assume a surface emissivity ϵ. We perform our analysis~~ The radiative transfer simulations were performed with two different ~~emissivities, one~~ surface emissivities ϵ. In the first set of simulations, ϵ is equal to 0.6, which corresponds to an ocean surface~~, and one~~. In the second set of simulations, ϵ is equal to 0.9, which corresponds to a land surface. ~~We furthermore assume specular reflection~~ Further, specular reflection is assumed. One should keep in mind though, that in reality ϵ depends strongly on the specific surface and to a smaller ~~extend also~~ extent on the channel~~channel~~. However, the results differ only little for the different emissivities. Therefore, we use the simplified assumption of a constant emissivity for all channels, and the main part of the results ~~we show~~ shown in this article will be for the emissivity of the ocean, i.e., $\epsilon = 0.6$.

3 Microphysical parameterisations

3.1 ICON

ICON uses the two-moment microphysical scheme by Seifert and Beheng (2006), which offers more detailed information about the cloud microphysical properties than the commonly used one-moment bulk schemes. It simulates the mass mixing ratio (M) and number mixing ratio (N) of cloud liquid water, cloud ice, rain, snow, hail and graupel. Since only very little graupel and hail was found in the simulation, we disregard them in the following. For the atmospheric radiative transfer simulator ARTS (Sect. 2.2) ~~we converted~~ the mass mixing ratios (unit kg kg^{-1}) were converted to mass densities (kg m^{-3}) by multiplying with the density of the atmosphere.

In the following, we refer to liquid cloud water mass density (liquid water content) as LWC, to cloud ice mass density as IWC, to rain mass density as RWC and to snow mass density as SWC. We ~~call the different types hydrometeors, and~~ refer to LWC and RWC as liquid hydrometeors and to IWC and SWC as frozen hydrometeors. The respective column integrated quantities, i.e. the paths, are denoted as LWP (cloud liquid water path), IWP (cloud ice water path), RWP (rain water path) and SWP (snow water path). Note that even though the ICON model's microphysical parameterisation requires a clear distinction between suspended and precipitating hydrometeors in each grid box, i.e., between LWC and RWC or IWC and SWC respectively, this

[2]See www.radiativetransfer.org for documentation and download.

Table 1. Distribution parameters for the hydrometeor particles after Seifert and Beheng (2006) and pers. comm. Seifert, 2014.

Hydrometeor type	ν	μ
LWC	1	1
RWC	0	1/3
IWC	0	1/3
SWC	0	1/2
Graupel	1	1/3
Hail	1	1/3

distinction can not be made in reality. Nevertheless we will discuss the cloud and precipitating hydrometeors separately in the remainder of the article, always keeping in mind that in reality, there is a smooth transition between the cloud ~~hydrometeors and the precipitating hydrometeorsand they can not easily be separated~~and precipitation hydrometeors.

For the simulation of the cloud radiative effect the size distribution and shape of the hydrometeors ~~is of~~ in terms of the mass-dimension relationship are of high importance. It is crucial to match the microphysical parameterisations of the radiative transfer model with those of the atmospheric model~~. The~~ , especially the size distribution.

The size distribution in the two-moment scheme ~~from Seifert and Beheng (2006)~~ by Seifert and Beheng (2006) is based on the hydrometeor mass. It employs a modified Γ-distribution with two free parameters as particle size distribution functions for each hydrometeor type. It is defined as:

$$f(m) = A\, m^{\nu} \exp\left(-\lambda m^{\mu}\right), \tag{1}$$

where the independent size parameter is the particle mass m. The distribution parameters are A, ν, λ and μ and have to be provided by the scheme. In the actual version of Seifert and Beheng (2006)'s scheme, ν and μ are fixed for each hydrometeor type (Table 1) and A and λ are calculated prognostically (see Seifert and Beheng (2006) for details of the calculation).

The size distributions from the two moment scheme for an idealised mean profile (purple) and a set of 90 individual ICON profiles (grey) are shown in Fig. 1 (for the definition of the idealised and the 90 profiles please refer to Sect. 5.2). Note that the distributions are height dependent. They are shown at a height of 550 hPa, where both ~~,~~IWC and SWC exist in considerable amounts. The curves illustrate the sum of the distributions for IWC and for SWC, i.e., all frozen hydrometeors. For the mean profile, also the individual distributions for IWC and SWC are shown to illustrate to what extent they overlap. The two peaks, which are evident in the idealised and in some of the 90 profiles, result from the two different types of frozen hydrometeors. The one at smaller diameters belongs to IWC, the one at larger diameters belongs to SWC. ~~It is important to note that in the~~ As opposed to one-moment schemes, in which the distinction between IWC and SWC is done through a size threshold, in the two-moment scheme the distinction between IWC and SWC is done via the processes a particle has undergone. A particle is counted as snow if it has~~for example~~ , for example, collided and joined with other hydrometeors (e.g. self-collection or collection of smaller hydrometeors). Single ice crystals are counted as cloud ice. Therefore, in the two moment-scheme cloud ice hydrometeors can be quite large in mass equivalent diameter and overlap with snow.

~~For comparison, the respective size distributionswhich result from McFarquhar and Heymsfield (1997) are also shown in Fig. 1. Note that the McFarquhar and Heymsfield (1997) parameterisation is based only on the mass densities of the hydrometeors, i.e., it is a one-moment parameterisation. Also, the scheme employs a common distribution of IWC and SWC instead of separate ones as used in the two-moment scheme. In the one-moment scheme, the distinction between IWC and SWC is done by setting a threshold for the size. For example, a frozen hydrometeor in McFarquhar and Heymsfield (1997) is counted as snow (large ice particle)if its mass equivalent diameter is larger than 100 m.~~

~~In the one-moment scheme, the largest snow hydrometeors are little bit smaller smaller than~~ It is noteworthy that different schemes provide different size distributions. Compared to, for example, frozen hydrometeor size distributions for tropical cirrus clouds by McFarquhar and Heymsfield (1997) (not shown), in the two-moment scheme ~~and the distribution is not as steep for large particles. But the possibly most important difference of the size distributions from McFarquhar and Heymsfield (1997) and Seifert and Beheng (2006) stands out in particular: The~~ the number densities for small ~~frozen hydrometeors in the two-moment scheme is~~ ice particles are orders of magnitude smaller~~than the one for the one-moment scheme. In this example~~. Apart from the different meteorological situation, this is mainly due to the fact that processes creating small ice particles in the two-moment scheme are missing (pers. comm. Axel Seifert, 2016).

~~Altogether the differences in the size distributions of the different approaches have a large impact on the radiative transfer calculations because the hydrometeor size strongly influences the scattering properties of the particles. Nevertheless the size~~

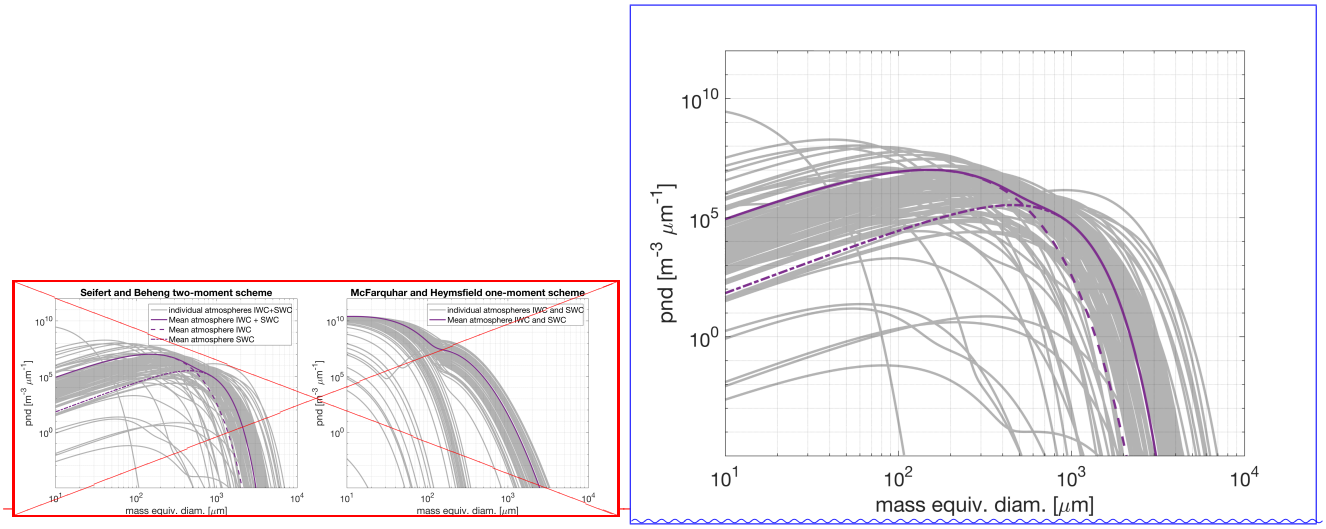

Figure 1. Size distributions for the idealised mean profile (purple) and 90 simulated profiles (grey) derived from ICON ~~(left) and from the parameterisation by McFarquhar and Heymsfield (1997) (right)~~ at 550 hPa each. ~~For the two moment scheme the~~ The sum of the distributions for IWC and SWC is shown for all profiles, and the individual distributions for IWC (~~dash-dotted~~dashed) and SWC (~~dashed~~dash-dotted) are shown for the mean profile.~~For the McFarquhar and Heymsfield scheme, the distribution for the sum of IWC and SWC is shown. The number density is ignored in this parameterisation. No individual distributions for IWC and SWC exist in that case. The same IWCs and SWCs stemming directly from the ICON simulation and at the height 550 hPa have been used in both cases.~~

distributions lie in a realistic equivalent diameter range compared to measurements. AlsoHowever, aircraft measurements have been criticised for having too many small particles due to shattering (e.g. Heymsfield, 2007) and the exact amount of smaller particles remains uncertain. However, for For the millimetre and sub-millimetre range this is not critical because the sensitivity to particles smaller than 100 µm is small in this range (Eriksson et al., 2008). For the benefit of a second prognostic moment, namely the number density, and the potential of having both to also retrieve microphysical parameters we stay with the two-moment scheme.

It should be noted that beside the differences in the size distribution also the parameterisation of the particle shape mass-dimension relationship is a crucial ingredient for radiative transfer modeling (e.g. Eriksson et al., 2015). However, atmospheric models normally only implicitly assume such a relationship, for example to parameterise collision or fall speeds. Also, normally atmospheric models have no detailed information about the particle shape. A Furthermore, different ice habits within one hydrometeor type (cloud ice, snow, hail, or graupel) are not considered. This will introduce some errors in both the microphysical calculations of ICON and the radiative transfer simulations. A perfect matching of the atmospheric model and the radiative transfer model with regard to this quantity particle shape and habit would require more sophisticated assumptions in the atmospheric model.

3.2 ARTS

The hydrometeor size distributions of the particles have been implemented in a discretised form into ARTS using the same distribution function as the two-moment scheme from Seifert and Beheng (2006). As a second variable representing the microphysical characteristics of the hydrometeors we chose the particle mean mass $\bar{m}$ and calculate it was chosen. It was calculated by dividing the mass mixing ratio M from ICON by the number mixing ratio N, both taken from ICON. This has the advantage that the mass density Jacobians for a fixed particle mean mass (as opposed to a fixed particle number mixing ratio) correspond to the ones one would get from a one-moment bulk scheme. However, in the remainder of the article we will focus on the mass densities and only include the values for the mean particle masses $\bar{m}$ in the final results for the information content to see if the channels higher than 183 GHz (see Sect. 5.1 for chosen set of channels) have a potential to measure cloud microphysical parameters such as hydrometeor size.

The scattering properties for the different hydrometeor types are defined as in Geer and Baordo (2014). For LWC and RWC we assume spherical particles spherical particles are assumed, for IWC soft spheres with a density of 900 kg m^{-3} are assumed. For spherical particles we calculated the single scattering properties were calculated with Mie theory, using the program by Mätzler (2002).

For SWC, the scattering properties were taken from the database of Liu (2008) assuming sector-like snowflakes for channels up to and including 334 GHz and the data base of Hong et al. (2009) assuming aggregates for channels higher than that. Since the original Hong et al. (2009) database assumes a constant effective density for the aggregates and also is is also based on the old earlier Warren (1984) refractive index we use a corrected version of the database, in which the absorption is rescaled using the Mätzler (2006) parameterisation for the refractive index of ice. Rescaling is done by multiplication with $\mathrm{imag}(n)/\mathrm{imag}(n_0)$, where n and n_0 are the refractive indices from Warren (1984) and Mätzler (2006), respectively. We apply the The rescaling to

obtain data for 183, 213, 243 and 266 K was applied. The scattering extinction and the phase matrix remain unchanged, which means that the rescaling only applies to the absorption (see Brath et al. (2018) for details).

We use the Discrete Ordinate ITerative (DOIT, (Emde et al., 2004)) method to calculate the scattering within ARTS. ~~We calculate the~~ The Planck brightness temperatures were calculated for all side bands within ~~our~~ the chosen set of channels (see Sect. 5.1). We do not use an explicit sensor response function but perform monochromatic radiative transfer simulations for the center frequencies of the side bands in each channel and use the mean of the two brightness temperatures. ~~We use a~~ For clear sky, highly resolved (in terms of frequencies) tests showed that the error compared to this simplified treatment is less than 1 K (Brath et al., 2018). Because the scattering properties of the hydrometeors change only marginally within the band width, a further increase of this uncertainty in the cloudy case is unlikely. A pencil beam with an incidence angle of 65° at the ground was used. For gas absorption we use the HITRAN (HIgh-resolution TRANsmission molecular absorption, Rothman et al. (2013)) database, the MT_CKD model (Mlawer et al., 2012) version 2.52 for the continuum absorption of water vapour and the MT_CKD model version 1.00 for the continuum absorption of oxygen.

4 Reduction of degrees of freedom

In principle, an information content analysis quantifies the information that is ~~contained in~~ obtained from a measurement with a certain set of channels. The information leads to the reduction of the a priori error - the larger the information content, the larger the reduction. A quantification of the information is~~for example~~ , for example, possible through calculating the reduction of the degrees of freedom (ΔDOF) for the analysis compared to the a priori state, or through calculating the entropy S of the two states (e.g. Rodgers, 2000; Di Michele and Bauer, 2006). In this study we use the reduction of the degrees of freedom ΔDOF, which is defined by

$$\Delta\mathrm{DOF} = \mathrm{trace}\left(I - S_r S_a^{-1}\right), \tag{2}$$

with the unity matrix I, the a priori covariance matrix S_a and the a posteriori, or analysis error covariance matrix S_r. S_r is defined according to the optimal estimation method as the reciprocal sum of the a priori and measurement error S_y:

$$S_r = \left(S_a^{-1} + J^T S_y^{-1} J\right)^{-1}. \tag{3}$$

S_y is transformed from measurement space into state space with the transpose of the Jacobian J. We set the measurement error to 1 K for each channel and assume that it is uncorrelated between channels, therefore S_y is a diagonal matrix with 1 K^2 on the diagonal. ~~Our assumption on S_a is~~ Furthermore, a perfect forward operator is assumed, since the focus of this study is mainly the interdependency of the information content for different hydrometeors within the atmospheric column. More realistic choices for the error of the forward operator are discussed for example in Aires et al. (2018). The assumptions made for S_a are described further below in Sect. 4.2.

If the analysis error after the measurement is equally large as the a priori error before, ΔDOF is zero and no information was gained. The closer the analysis error is to zero, the larger ~~is~~ ΔDOF is, with a maximum (in reality unreachable) value equal to the number of channels, in our case 24. ΔDOF can also be interpreted as pieces of information. If we have ~~1~~ one piece

of information ~~we can retrieve 1 quantity~~ one quantity can be retrieved, for example the hydrometeor path~~, i. e., the column integrated mass of the hydrometeor.~~ . If we have two pieces~~we can get two quantities~~ , two quantities can be obtained, for example the hydrometeor mass in two different heights.

For ~~our analysis, we need~~ the analysis, the portion of the information content is needed, which is associated with the specific hydrometeors. The method we chose is a linear splitting of the trace in the definition of ΔDOF to the block matrices which correspond to the respective quantity (H2O, IWC, LWC, SWC, RWC and the respective hydrometeor mean masses). However, we would like to stress that this is an approximation and does not consider the cross-correlations between the various hydrometeors.

4.1 Jacobians

The calculation of the Jacobians by explicit perturbation (in contrast to the analytical calculation) J generally requires ~~the following steps: (1)~~ three steps: First, calculate the brightness temperature T_B^c for a specific channel c for the unperturbed atmosphere~~, (2)~~ . Second, perturb one atmospheric quantity x, for example IWC, by a perturbation δ and again simulate the perturbed brightness temperature $[T_B^c]_\delta$ for that channel~~, (3)~~ . Third, divide the difference of the two brightness temperatures by the perturbation. If, as in our analysis, height resolved Jacobians are required, the perturbation has to be applied successively to each of the height levels k. Note that a perturbation at a distinct height level k strictly ~~spoken~~ speaking means a perturbation of the respective quantity at the two adjacent height layers which the radiation passes through.

The Jacobian $J_{c,k}$ at height k and for a channel c is therefore given by:

$$J_{c,k} = \frac{[T_B^c]_{k,\delta} - T_B^c}{\delta}, \tag{4}$$

with $[T_B^c]_{k,\delta}$ as the simulated brightness temperature if ~~we perturb~~ the quantity x_k is perturbed, which denotes the value of x at the height level k.

For ~~our~~ the analysis, we define δ as a relative perturbation of x_k, as opposed to using an absolute value that is independent of the specific value of the x_k. This is especially useful for the calculation of Jacobians for the hydrometeor profiles. First, the values of x over height span several orders of magnitude. The use of a relative perturbation ensures that the perturbation is always small compared to the original value, and linearity can be assumed. Second, the hydrometeor profiles are discontinuous and do not exist at all heights. Using the relative perturbation ensures that ~~we only perturb~~ only that part of the profile where hydrometeors exist in the first place ~~. In our analysis, we~~ is perturbed. We use $\delta = 1\%$ for each quantity (including water vapour, which in the following is referred to as H2O) and at all heights.

Relative Jacobians also correspond to the retrieval of a quantity in logarithmic space. Regarding $1 + \delta$ as the development of the natural logarithm for small δ ~~we can find~~ it can be shown that $\delta = \ln(x_{k,\delta}) - \ln(x_k) = \Delta \ln x_k$, with x_k as unperturbed value at height level k and $x_{k,\delta}$ as perturbed value. The Jacobian then is

$$J_{c,k} = \frac{[T_B^c]_{k,\delta} - T_B^c}{\Delta \ln(x_k)}, \tag{5}$$

As stated above, this corresponds to a retrieval in natural logarithm space. In the remainder of the article, we will ~~entirely~~ stay in the framework of a logarithmic retrieval entirely.

~~We calculate the~~ The Jacobians for each of the two sidebands (see Sect. 5 for the definition of channels and side bands) ~~and use~~ were calculated and the mean of the two Jacobians was used for the subsequent analysis. We use the same height grid in ARTS as in the ICON simulation. ~~We calculated the~~ The Jacobians for the H2O volume mixing ratio (VMR), the hydrometeor mass densities M and the hydrometeor mean mass $\bar{m}$ were calculated. For the analysis, ~~we use the Jacobians~~ Jacobians were used in units of K/100% as calculated by ARTS. For the purpose of showing them in the following sections, they are normalised by the height layer thickness. Note that the height layers broaden with increasing height. This yields the unit K/(%·km), which appears in the plots. Thus ~~we ensure~~ the comparability of the Jacobians at different height levels is ensured. All calculations, however, have been performed on the unnormalised values.

Note that Eq. (4) and (5) only conceptually describe the Jacobian calculation. In practice, we do not make a fully independent T_B calculation for each perturbation, since this is computationally very inefficient for the iterative scattering solver used (Emde et al., 2004). Instead, the scattering solver ~~for the perturbations gets the reference result as a first guess, which saves most of the iterations that would otherwise be needed~~uses the result from the unperturbed scheme as a starting point. That result should be close to the result from the perturbed case already, because the profile perturbations are small. From that starting point, the perturbed Jacobians are calculated with far fewer iterations compared to a completely uneducated starting point, which makes the scheme far more computationally efficient.

4.2 A priori covariance

The final ~~ingredient~~ component necessary to calculate the information content of a measurement is the a priori covariance error matrix S_a. In ~~our~~ the ICON model framework ~~we have the opportunity to calculate that matrix directly out of~~ that matrix can be calculated directly from the model data as the covariance of the different quantities on different height levels. This means that we take the model mean state as a priori state, and the full variability of the model on the chosen domain (state domain) and simulation time as its uncertainty. ~~We have to keep in mind that the simulation case is a spring day in the mid-latitudes and that the variability is therefore limited. In reality,~~

Certain assumptions have to be made in order to calculate the a priori covariance. First, only cloudy cases are considered. We assume that some kind of cloud detection has been done prior to the observation of the cloudy sky. To identify cloudy cases in the model, a threshold for the total condensed water path is applied, i.e., for the sum of the paths of all hydrometeors. We use the approximate detection threshold of $10^{-4}\,\mathrm{kg\,m^{-2}}$. If the total water path exceeds that threshold, the ~~inter-seasonal and also the inter-annual variability of the atmospheric conditions in the mid-latitudes would be even larger than what we get from our spring case. To cover the broadest possible statistics from this case, we use the entire three days of the model simulation.This especially means that we cover clear sky cases as well as frontal cases with our a priori assumption.We find that already in this limited case, the variability of the hydrometeors is very large (up to 670 in ln space). On the contrary, the variability of H2O is quite low (order of 1) because it corresponds more to the overall synoptic situation, which only changes on time scales of days.~~

~~Also, the dynamical range of H2O is smaller than the one for the hydrometeors. Note that since we use~~ corresponding profile is used in the calculation of the a priori error covariance.

Since relative Jacobians (see Sect. 4.1) were used, i.e. a retrieval in natural logarithm space, ~~we also need to calculate the covariance in ln-space~~also the covariance needs to be calculated in ln space. To enable this calculation, zero values ~~were treated by setting them to the smallest possible float difference (2.22e-16 in the respective unit).~~ have to be removed from the hydrometeor profiles. For this purpose we set a threshold for each quantity for which the a priori error covariance is calculated. The choice of this threshold is a non-trivial task, and the threshold will affect the desired information content. We will address this in more detail in the respective result section. The smaller the threshold is, the larger the a priori variance is and the more information an observation will provide in comparison.

H2O is smooth and, above all, continuous. Therefore the numerical model threshold $10^{-20}\,\mathrm{kg\,m^{-3}}$ is used for it. For the hydrometeor mass densities $10^{-7}\,\mathrm{kg\,m^{-3}}$ is used. If we assume a detection limit for the water path of $1\,\mathrm{g\,m^{-2}}$ and a cloud thickness in the order of 1 km, then this value for the local mass density is a little bit smaller than the detection limit, depending on the real cloud thickness. Furthermore, that mass density threshold value is close to an internal threshold within the two-moment microphysics scheme (close, because the microphysics scheme employs mixing ratios instead of mass densities). For example, if the mass density of cloud ice is larger than that threshold, collisional growth can take place (pers. comm. Axel Seifert, 2017). For the mean masses of the different hydrometeors, separate minimum values are used in the two-moment scheme. The thresholds employed are $4.2{\cdot}10^{-15}\,\mathrm{kg}$ for cloud liquid water mean mass, $10^{-12}\,\mathrm{kg}$ for cloud ice mean mass, $2.6{\cdot}10^{-10}\,\mathrm{kg}$ for rain mean mass, and $10^{-10}\,\mathrm{kg}$ for snow mean mass. The same thresholds for the mean masses were used in the calculation of the a priori error covariance. The chosen thresholds furthermore ensure that the relevant peaks, within the mass density distributions for LWC, RWC, IWC and SWC, which constitute the clouds or precipitation, are covered. The peaks are roughly located at -4.2 with a width of 0.7 in units of the decadal logarithm (LWC), -5.3 with a width of 0.8 (IWC), -5.0 with a width of 0.8 (RWC) and at -5.3 with a width of 0.9 (SWC). Therefore they are all well above 10^{-7}, which was chosen as threshold. Because for the mean masses we used the model inherent thresholds for the distribution, this is naturally true for the mean masses of all hydrometeors as well (not shown). We are aware that those choices affect the results for the information content. It will be discussed further in Sec. 6.3.

Figure 2 shows the a priori covariance in ln space and the corresponding correlation matrix defined as $C_{i,j} = S_{i,j}/\sqrt{S_{ii}S_{jj}}$. The 25 block matrices give the covariance and correlation of pairs of model variables on their 49 height levels. Note that we have to skip the uppermost 50th height level from ICON because ARTS requires one level on top of the "cloud box" which defines the cloudy area where scattering is calculated. Since the matrices are symmetric, only the lower triangle is shown for clarity.

The covariance naturally is largest at the height levels where hydrometeors reside and goes up to ~~670~~ 12.2 in units of the natural logarithm on the diagonal of the ~~SWC~~LWC×~~SWC~~ LWC block matrix. For the other hydrometeors, the maximum reaches almost up to eight on the diagonal. The covariance for ~~LWC with itself is comparably small. The one for~~ H2O is ~~smooth and the spread of values is very~~ small compared to the one for hydrometeors (~~order of 1~~smaller than one). This reflects the much lower variability and smaller dynamical range of H2O compared to hydrometeors. Note that the ~~regarded scene~~

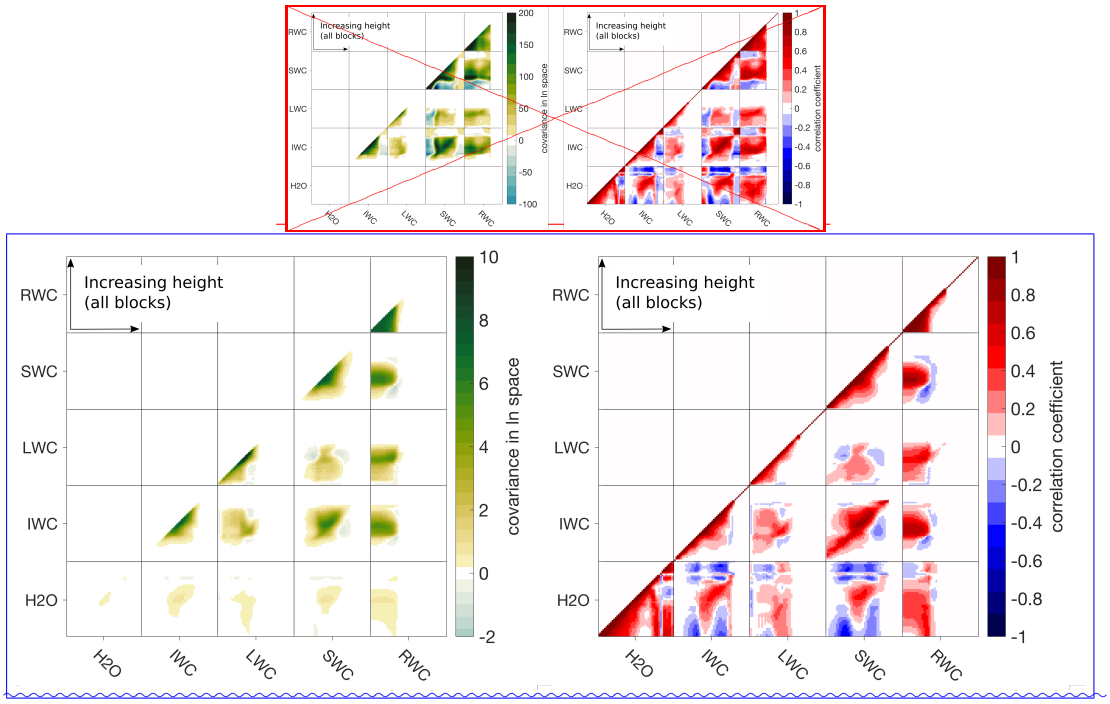

Figure 2. A priori error covariance (left) and the corresponding correlation matrix (right). Only the lower triangle is shown for clarity, since the matrices are symmetric. The block matrices correspond to the (auto-)correlation for one or between two quantities. They have the dimension of 49×49 height levels each, the height increases within the blocks from left to right and from bottom to top. Note that the variability of H2O is so small in comparison to the hydrometeors (in the range of 0 to 1) that ~~it cannot~~ only little covariance can be seen in the a priori covariance (left) due to the scaling.

scene investigated is a short period ~~spring time front~~ in spring time in the mid-latitudes. In ~~winter, the correlations likely will~~ other seasons, the a priori covariance will likely look different, ~~when snow for example reaches the ground~~ especially for the hydrometeors. In winter, for example, snow can reach the ground and there would be a non-zero covariance down to the ground.

There is a rich structure of autocorrelations and correlations between different hydrometeors and over different height levels. ~~For example, the autocorrelation for SWC is positive in the upper layers but negative for a combination of upper and lower levels. This is also seen in the correlation of~~ The autocorrelation for the different hydrometeor types is mostly positive everywhere, which accounts for the thickness of the cloud layer and the falling precipitation. For SWC and RWC, ~~which are anti-correlated at lower levels. The autocorrelation for RWC is entirely positive below~~ for example, the correlation in the upper layers is negative. This may be interpreted in terms of the melting layer~~, and zero above, where rain does not exist. This is due to the prognostic rain falling down through the different height levels over time. This means, in order to have precipitation in lower levels it needs to be present in the upper levels in~~ . Above the melting layer snow exists. It melts below the melting layer forming rain. Therefore precipitating snow in the ~~first place in order to fall down~~upper layers will lead to rain in heights below the melting layer.

In the correlation plot also ~~the structures for~~ rich structures within the H2O related blocks become evident. ~~It~~ H2O is positively correlated with hydrometeors within the clouds and precipitation regions, since the atmosphere is near saturation there. The negative correlation at lower regions may be due to ~~the fact that in case hydrometeors are present in~~ evaporation in sub-saturated regions~~evaporation takes place which decreases~~ . Here, the hydrometeor mass ~~but increases~~ decreases and the H2O mass increases. At higher regions above the clouds it may be spurious and stem from the fact that there are only numerical artefacts of very small amounts of hydrometeors in comparison to realistic amounts of H2O.

The covariance and correlations ~~stem~~ were calculated on the basis of 1.8 million near-realistic cloudy profiles from the ICON model simulation~~, i. e., from about 300 000 near-realistic profiles. With the ICON matrix~~ . With this covariance and correlation from ICON data, we automatically get the cross-correlations for the different hydrometeor types ~~and do not have to add additional assumptions~~as well. However, one has to be aware that there are model inherent correlations due to the microphysical parameterisation, which can cause some artefacts. ~~Also, the~~ Furthermore the choice of thresholds to remove the zero values in the profiles scales the covariance and therefore will affect the information content. The terrain following coordinates of ICON cause slightly larger covariances in the lower levels for H2O and rain, which ~~both are~~ are both present near the ground. Idealised covariance matrices might be constructed instead (e.g. Aires et al. (2018)), but they have different ~~flaws as well and contain many more or less arbitrary~~ downsides and also contain many assumptions, especially for the cross-correlation of hydrometeors. We therefore chose the model based a priori covariance matrix to perform ~~our~~ the study, keeping in mind the downside that the model introduces some artificial correlations between the hydrometeors.

5 Setup

5.1 Channels

~~In our analysis, we use radiometer~~ Radiometer channels as applied on the International Sub-millimeter Microwave Airborne Radiometer (ISMAR, Fox et al. (2017)) and on the Microwave Airborne Radiometer Scanning System (MARSS, McGrath and Hewison (2001)) are used. Both were ~~employed in~~ deployed on a recent flight campaign (Brath et al., 2018) and cover channels from 89.0 GHz up to 664.0 GHz. ISMAR will be extended with a channel at 874.4 GHz in near future. They include the AMSU-B channels and the ICI setup, with the exception that the ICI-1, ICI-2 and ICI-3 channels have a slightly different distance from the H2O absorption peak at 183.31 GHz (Pica et al. (2012)). We will later use the three 183.31 GHz channels from MARSS instead. ~~We further complement the setup~~ The setup is further complemented by two channels at 23.8 and 50.1 GHz from the Dual-frequency Extension to In-flight Microwave Observing System (Deimos, Hewison (1995)) to account for lower frequency precipitation channels, which are also part of MWI. The resulting set of channels, their side bands, and the respective instrument they belong to is given in Table 2.

With this setup it is possible to investigate the principle interdependencies of the information content on different hydrometeors from a set of channels, which is capable ~~to observe~~ of observing liquid and frozen cloud as well as precipitation hydrometeors. But it is also possible to put a special focus on the upcoming ICI instrument on MetOp-SG, which employs channels from 183 GHz ~~upwards to~~ up to 664.0 GHz to gain more detailed information about cloud ice, its microphysical properties, and

maybe even some more profile information than the instruments that are currently ~~employed~~ deployed in the different satellite missions.

Table 2. Selected set of channels from the instruments MARSS, ISMAR and Deimos. Channels equal or similar to the ones of the MetOp-SG mission (ICI and MWI) are marked in the right column.

Center frequency [GHz]	Side bands [GHz]	Bandwidths [GHz]	Instrument	METOP-SG
23.8	±0.07	0.127	Deimos	MWI-2
50.1	±0.08	0.082	Deimos	near MWI-4
89.0	±1.1	0.65	MARSS	MWI-8
118.75	±1.1	0.4	ISMAR	near MWI-12
118.75	±1.5	0.4	ISMAR	near MWI-11
118.75	±2.1	0.8	ISMAR	near MWI-10
118.75	±3.0	1.0	ISMAR	near MWI-9
118.75	±5.0	2.0	ISMAR	
157.05	±2.6	2.6	MARSS	
183.31	±1.0	0.45	MARSS	near ICI-3
183.31	±3.0	1.0	MARSS	near MWI-17, near ICI-2
183.31	±7.0	2.0	MARSS	near ICI-1
243.20	±2.5	3.0	ISMAR	near MWI-18, ICI-4
325.15	±1.5	1.6	ISMAR	ICI-7
325.15	±3.5	2.4	ISMAR	ICI-6
325.15	±9.5	3.0	ISMAR	ICI-5
424.70	±1.0	0.4	ISMAR	
424.70	±1.5	0.6	ISMAR	
424.70	±4.0	1.0	ISMAR	
448.0	±1.4	1.2	ISMAR	ICI-10
448.0	±3.0	2.0	ISMAR	ICI-9
448.0	±7.2	3.0	ISMAR	ICI-8
664.0	±4.2	3.0	ISMAR	ICI-11
874.4	±6.0	3.0	ISMAR	

5.2 Atmospheric profiles

To facilitate the analysis ~~we have calculated~~ a mean profile (Fig. 3) from 10 000 ICON profiles, which each are amongst the extremes for one specific hydrometeor or the humidity~~. To chose them, we calculated~~ , was calculated. To choose the 10 000 profiles, the hydrometeor paths for each hydrometeor type and each atmospheric ~~column~~profile were calculated. To exclude

~~outliers we disregard the columns with a~~ unphysical outliers, which may be produced by the model, profiles with a hydrometeor path larger than the ~~99th percentile . For the rest of the columns~~ 99th percentile were disregarded. From the remaining profiles we chose 10 000/7 largest ~~paths for~~ H2O ~~, LWC, IWC, RWC, SWC,~~ paths, LWPs, IWPs, RWPs, SWPs, and the paths for hail and graupel (the "divided by seven" stems from the ~~7 quantitieswe loop over~~ seven quantities, over which the loop is done). This ensures that a considerable amount of each hydrometeor, except for hail and graupel, which ~~do only consist~~ only exist in very small amounts over the whole simulation, is contained in the profile. However, since the 10 000 atmospheres are not required to be extreme with regard to or contain all hydrometeor types at once, this gives us 10 000 cloudy profiles and on average a mean profile which is not extreme for any hydrometeor and which is comparably smooth. ~~This~~ The mean profile that follows from these choices contains realistic amounts of hydrometeor masses~~and cloud and~~ . Cloud and precipitation are located in physically reasonable height ranges. ~~It~~ However, it has to be kept in mind ~~, though,~~ that this may lead to an unlikely combination of hydrometeors, such as LWC and SWC being present in the same atmospheric column. Therefore, in Sect. 6.4, we will also show results from a set of 90 individual cloudy atmospheric columns drawn directly from the selected ICON simulation to consolidate the results from the idealised atmosphere.

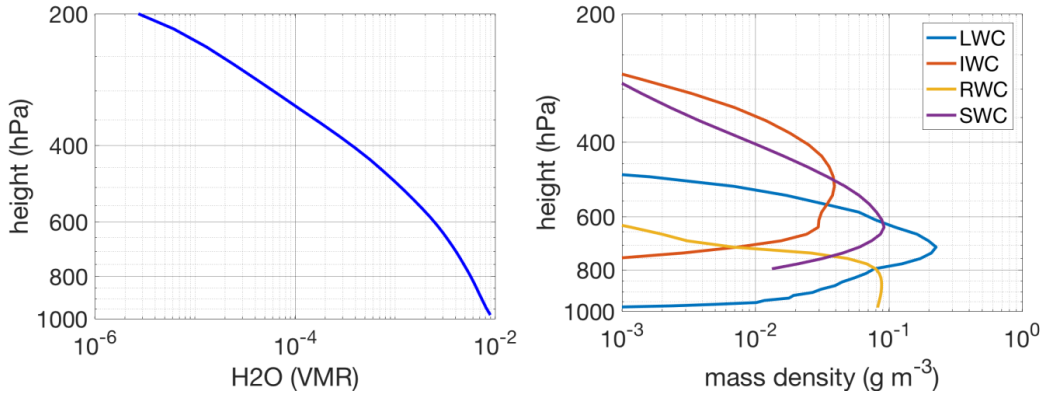

Figure 3. Idealised atmospheric base profile. H2O volume mixing ratio (VMR, left) and particle mass densities (right) for LWC, IWC, RWC and SWC. The respective paths are LWP=0.45 kg m^{-2}, IWP=0.17 kg m^{-2}, RWP=0.18 kg m^{-2}, SWP=0.30 kg m^{-2} and H2O path=25.00 kg m^{-2}.

~~We use this mean profile~~ This mean profile is used as a "base profile" containing all hydrometeors. From this base profile ~~we create~~ atmospheres with different combinations of cloud hydrometeors are constructed by taking out or putting in specific hydrometeors. A similar approach has been used by Guerbette et al. (2016), who progressively put in cloud hydrometeors to quantify their respective influence on the brightness temperature in the 183 GHz channel of the humidity sounder SAPHIR on Megha-Tropiques. ~~In our study , we investigate~~ This study investigates if the information about one hydrometeor type depends on the presence of another. For example, we can have an atmosphere which contains only LWC or only IWC, or one which contains the two hydrometeor types IWC and RWC. All in all 16 combinations including ~~the~~ clear sky are possible. We are aware that not all combinations are physically possible and realistic, such as an atmosphere only containing SWC, but we

want to understand how the measurement of one hydrometeor is in principle influenced by the others. Therefore ~~we regard~~ all mathematically possible combinations are regarded.

~~We denote the different atmospheres~~ The different atmospheres are denoted by an a_X, where X contains the composition of the atmosphere. LWC is denoted by L, IWC by I, RWC by R and SWC by S. For example, the atmosphere containing IWC and LWC is called a_{IL}. The clear sky case ("Vapour") is called a_V. Note that H2O is present in all of the atmospheres, even though it is not explicitly included in X in case hydrometeors are present. An overview over the atmospheric compositions is given in Table 3.

6 Results

6.1 Brightness temperature spectra

The brightness temperatures for the different atmospheric compositions are shown in Fig. 4 for an emissivity of $\epsilon = 0.6$. ~~Naturally, the~~ The brightness temperature spectra differ ~~for the different atmospheric compositions, and they differ~~ by up to 80 K, depending on the atmospheric composition and the measurement channel. In the window channels, the spread in the spectra is particularly large, while in the sounding channels near the absorption peaks the spread is smaller. For channels close to absorption line centres the spectra almost lie on top of each other because here the atmosphere is opaque due to H2O absorption. Some of the different compositions such as a_L and a_{LR} or a_{IS} and a_{IRS}, have almost the same spectra except for differences in the window channels below 118.75 GHz~~, which~~. This implies that some hydrometeors are invisible to channels higher than that~~, e. g. due to the high opacity of the~~.

The brightness temperature is a result of the complex interaction of the radiation with the atmosphere. First, there is extinction, i.e., absorption, mainly caused by H2O ~~, which shields hydrometeorsin lower atmospheric levels or due to a general insensitivity~~ and by the liquid hydrometeors and scattering, mainly caused by the frozen hydrometeors. Extinction determines how far down a certain channel can see. This also determines the sensitivity of a channel to an atmospheric component to some degree. If the channels do not reach down to levels where, for example, rain exists, naturally it is not sensitive to rain in that case. The whole hydrometeor path of a certain hydrometeor, which is in the pathway of the channel~~to the respective hydrometeor~~

Table 3. Atmospheric compositions used in the analysis of the dependency of the information content on the atmospheric composition.

		Atmosphere															
		a_V	a_L	a_R	a_I	a_S	a_{LR}	a_{LI}	a_{LS}	a_{RI}	a_{RS}	a_{IS}	a_{LRI}	a_{LRS}	a_{LIS}	a_{RIS}	a_{LRIS}
Hydrometeors	Vapour	X	X	X	X	X	X	X	X	X	X	X	X	X	X	X	X
	LWC		X				X	X	X				X	X	X		X
	RWC			X			X			X	X		X	X		X	X
	IWC				X			X		X		X	X		X	X	X
	SWC					X			X		X	X		X	X	X	X

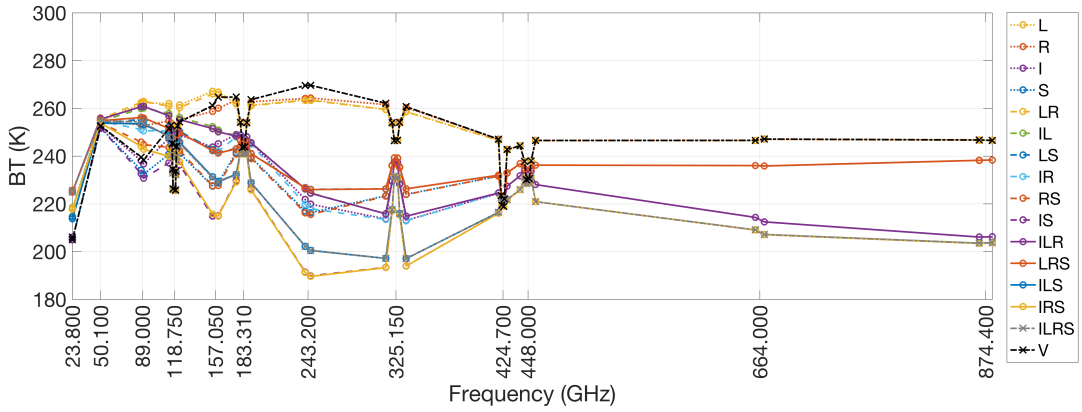

Figure 4. Brightness temperature spectrum for $\epsilon = 0.6$ for the 16 combinations of the base profile. The legend corresponds to the composition suffixes X defined in Table 3. The labels on the abscissa are the center frequencies of the channels. The curve labeled "V" is for H2O only, without any hydrometeors. Although not mentioned in the legend, vapour is also present in all the other calculations.

~~type. Hydrometeors~~ , contributes to the signal. It depends on the respective path of the hydrometeor and the sensitivity of the channel to that hydrometeor how big the contribution is. If we look at one particular hydrometeor, the combined signals of all other atmospheric components provide the radiative background for the signal of that particular hydrometeor. This may lead to a "shielding" of hydrometeors in the lower levels, because the water vapor path or hydrometeor path above those hydrometeors is so large that the atmosphere is entirely opaque for a channel. The signal from a certain hydrometeor can also be ~~shielded~~ masked by other hydrometeors, that create a radiative background through absorption or scattering, which is similar to the radiative signal of the hydrometeor in question~~, which masks the signal~~. In the following we investigate this further. We will have a closer look at the sensitivities of the brightness temperature to changes in the hydrometeor mass, namely the Jacobians J, in the absence and presence of other hydrometeors.

6.2 Cloudy Sky Jacobians

We first look at the Jacobians for H2O for the clear sky case a_V and the all-hydrometeors case a_{ILRS} are analysed (Fig. 5). H2O has the advantage that its profile is smooth and continuous, contrary to the hydrometeor Jacobians which per definition of the relative perturbation only exist where the cloud hydrometeors reside and which decrease to zero at the cloud edge with a steep gradient. With the chosen surface emissivity of $\epsilon = 0.6$, for a_V, H2O gives a warming signal from the lower atmosphere (> 500 hPa) at channels from 157.05 GHz downward and at 243.2 GHz. For channels from 183.31 GHz upward it gives a small cooling signal at higher levels (< 650 hPa). Hereby "warming signal" ("cooling signal") ~~in our context~~ means that an increase of the amount of vapour or hydrometeor content leads to a warming (cooling) of the resulting brightness temperature at the top of the atmosphere. This is mainly due to the fact that the Jacobians for the sounding channels higher than 183 GHz peak

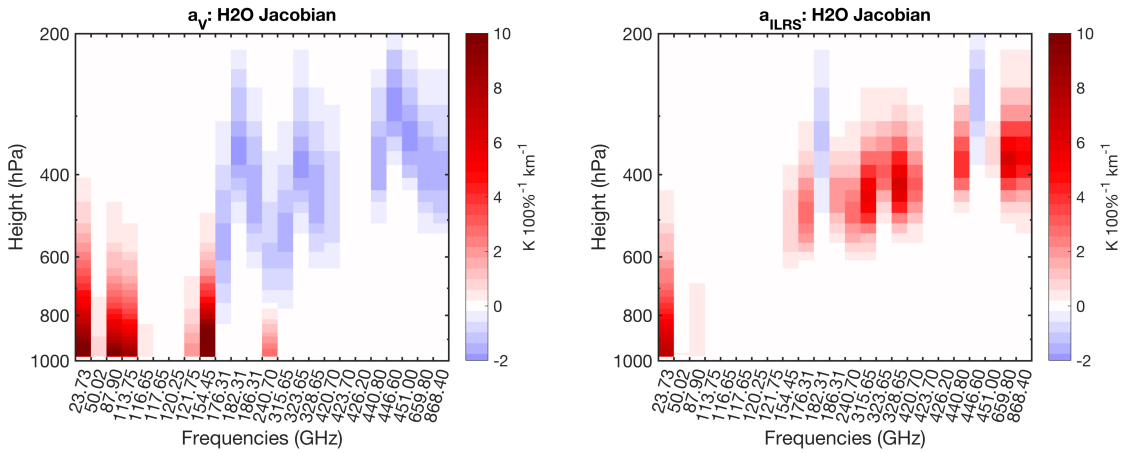

Figure 5. H2O Jacobians for the clear sky case a_V (left) and for the all-hydrometeor case a_{ILRS} (right) for an emissivity $\epsilon = 0.6$. Averages of the sidebands are shown, the labels on the abscissa denote the left sideband of the channel.

higher up in the atmosphere than the Jacobians of the lower channels and that these higher regions are very cold compared to the ground.

This picture changes dramatically in the presence of all considered cloud hydrometeors (a_{ILRS}). Except for the most central ~~ones~~ frequencies of the sounding channels at 183.31 GHz and 448.0 GHz the H2O signal in this case is entirely positive. The positive signal in between the channels at 157.05 GHz and 23.8 GHz decreases to almost zero. The sensitivity of the measured brightness temperature to changes in ~~the~~ H2O is highly dependent on the presence of clouds.

The H2O example illustrates the general principle of these interactions well~~:~~. If the radiative background is cold, then the presence of a scattering or absorbing species tends to increase the brightness temperature. Conversely, if the background is warm, then the species ~~tend~~ tends to reduce the brightness temperature. For H2O at high frequencies, the presence of frozen hydrometeors in the upper troposphere, which have a cooling signal due to scattering, turns the scene from a warm background case to a cold background case.

Figure 6 illustrates Jacobians from atmospheres with one single liquid hydrometeor type each, i.e., a_L and a_R for both, LWC or RWC, along with the corresponding H2O Jacobians. ~~Because we used a~~ As relative perturbation for the calculation of the Jacobians were used, (Eq. (5)), the cloud Jacobians ~~naturally~~ only exist at those heights where LWC or RWC exist (cp. Fig. 3). These heights are indicated in the figures for two different thresholds for the respective mass densities. Mainly the channels below 325.15 GHz (LWC) respectively 243.2 GHz (RWC) are sensitive to the liquid hydrometeors. The window channels at 23.8 GHz, 50.1 GHz and 89.0 GHz give a warming signal at all heights, the outermost channel at 118.75 GHz (and 157.05 GHz for RWC) have a warming signal at lower levels and a cooling signal at upper levels. Note that a higher surface emissivity, i.e., a radiatively warmer surface, reduces the warming signal from LWC and RWC in the window channels, since the surface provides a warmer background in that case (not shown). The Jacobians for H2O change in the presence of LWC or RWC.

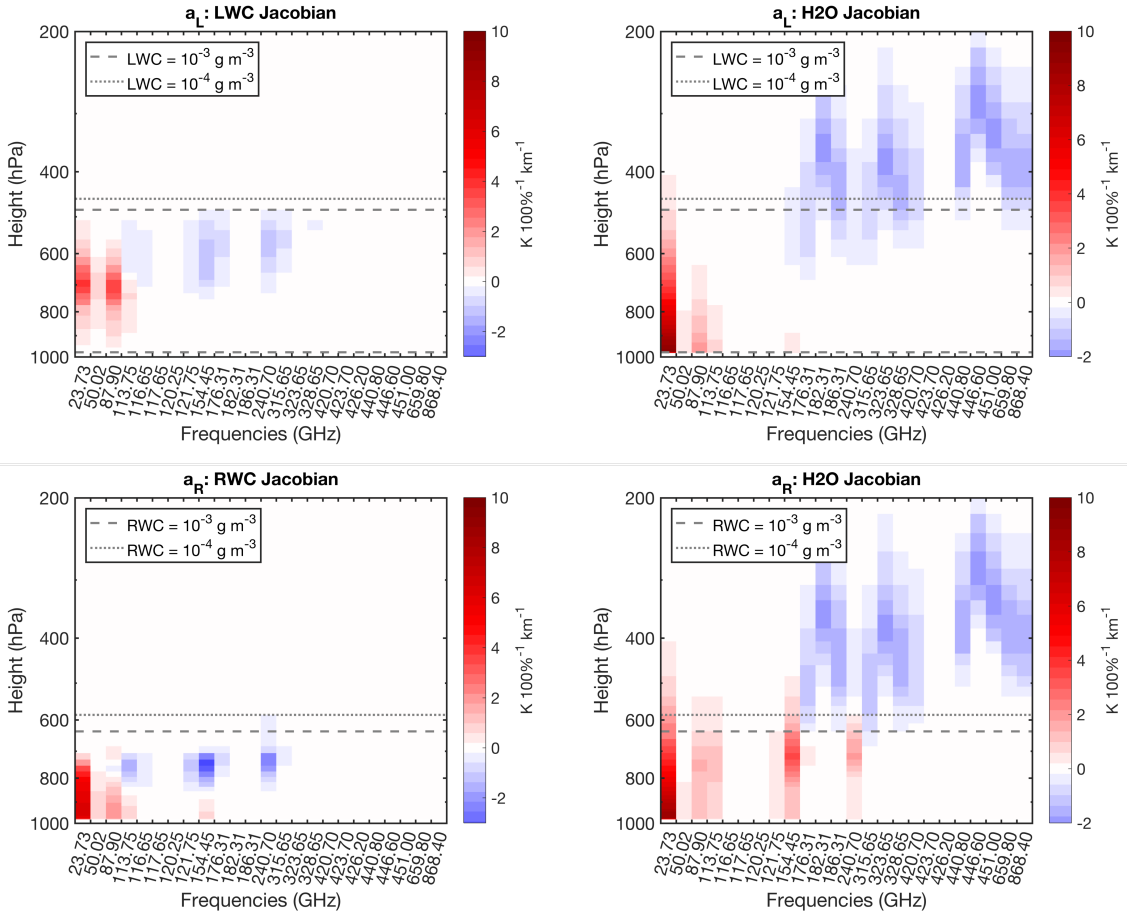

Figure 6. LWC (top left) and H2O (top right) Jacobians for a_L, RWC (bottom left) and H2O (bottom right) Jacobians for a_R ($\epsilon = 0.6$). The dashed (dotted) grey line denotes the height in which the mass content of the respective hydrometeor is nearest 10^{-3} g/m^3 (10^{-4} g/m^3). Note that both hydrometeor types reach far down to the ground such that the lower edges are not always visible in the plots.

Apart from 23.8 GHz the warming signal in the lower channels is considerably reduced ~~. The~~ compared to the warming signal from H2O alone~~is partly shielded by the warming signal from LWC and RWC~~.

The frozen hydrometeor types IWC and SWC generally give a cooling signal (Fig. 7) since they mainly act as scatterers rather than absorbers in the selected channel range. Also, they exist at low ambient temperatures, and even their emission would cause a cooling signal. The upper channels above 157.05 GHz are sensitive to these hydrometeor types. For SWC a considerable signal also comes from the channels at 50.1, 89.0 and the outermost 118.75 GHz channel. The highest channels at 664.0 and 874.4 GHz are more sensitive to IWC than to SWC because the scattering efficiency in these two channels is larger for the smaller ice hydrometeors than for the larger snow hydrometeors.

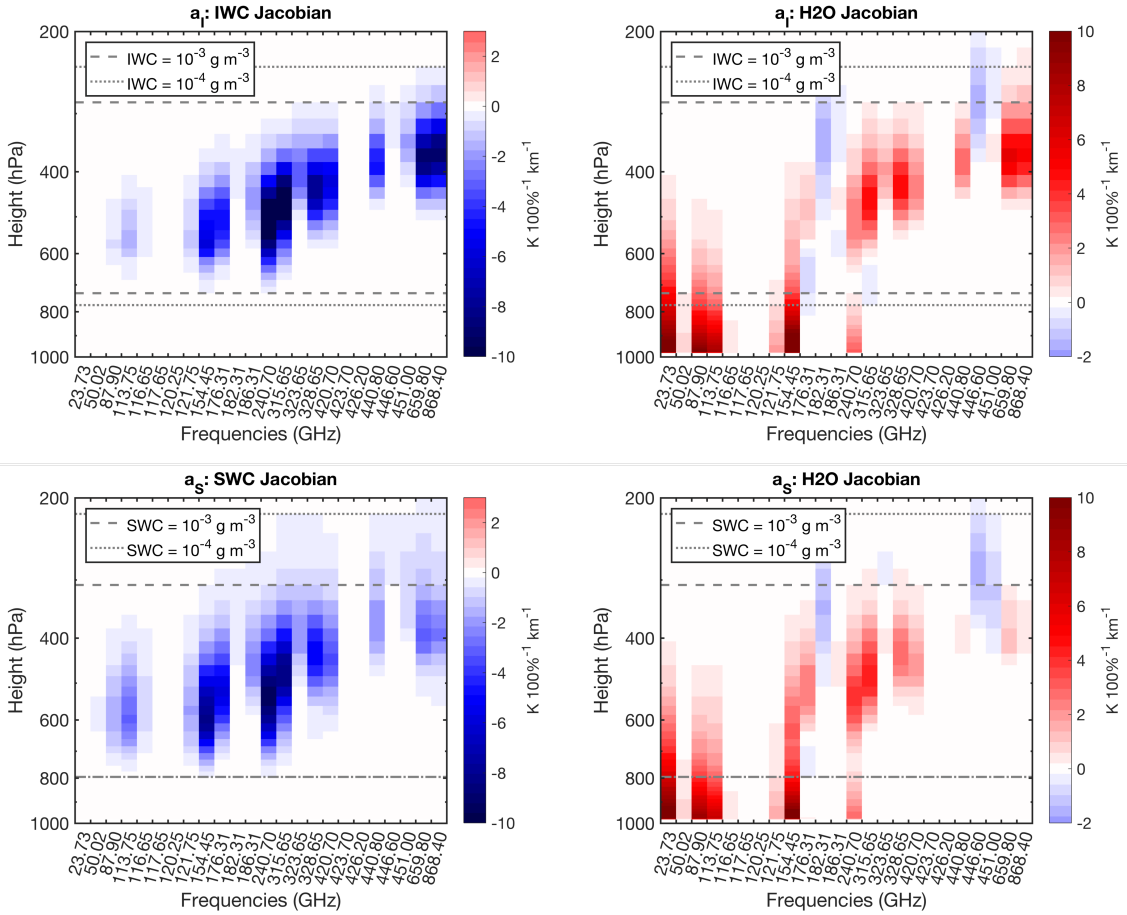

Figure 7. Same as Fig. 6 but for IWC (top) and SWC (bottom).

The corresponding H2O Jacobians are considerably changed at channels above 157.05 GHz~~:~~. The cooling signal from the clear sky H2O Jacobians (Fig. 5) is turned into a warming ~~one~~ signal except for the sounding channels closest to the absorption lines. This is in accordance with the findings of Guerbette et al. (2016) who found such a change of sign in the lowest-peaking SAPHIR channels near 183 GHz in the presence of high concentrations of snow above 500 hPa.

Next, we will go deeper into the interdependencies of the hydrometeor Jacobians. For this purpose, ~~we reduce~~ the view chosen in the previous figures is reduced, and only ~~show~~ the Jacobians for the channels at 89.0 ~~GHz~~ and 243.2 GHz are shown as line plots (Figs. 8 and 9). In these channels we expect to get a signal from all cloud hydrometeors, ~~although~~ while 89.0 GHz is more sensitive to the liquid hydrometeors and 243.2 GHz is more sensitive to the frozen hydrometeors. ~~We show the Jacobians~~ The Jacobians are shown for each cloud hydrometeor type for the cases where only that specific type is present, one other hydrometeor type is present, or all types are present in a combined plot. ~~At~~ For the example of cloud ice these are IWC Jacobians for the cases a_I, a_{IL}, a_{IS}, a_{IR}, and a_{ILRS}.

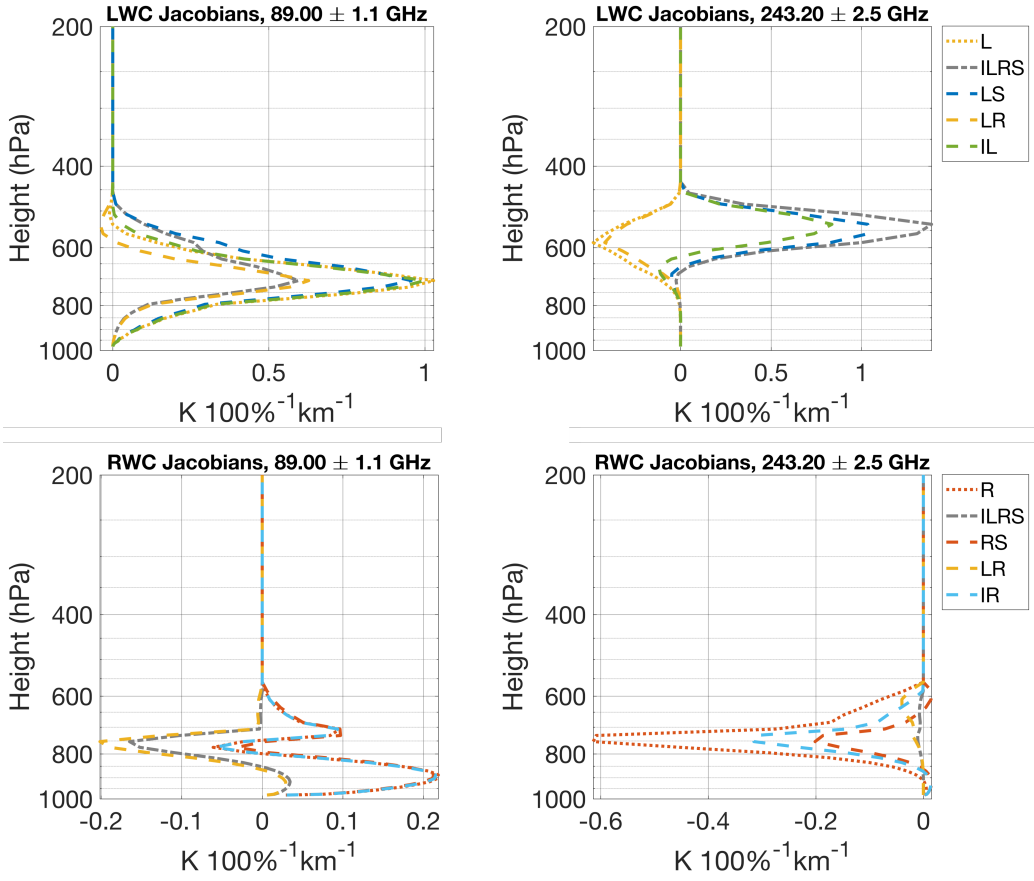

Figure 8. LWC (top row) and RWC (bottom row) Jacobians for the 89.0 GHz (left column) and the 243.2 GHz (right column) channel ($\epsilon = 0.6$). Shown are atmospheres containing pairs of hydrometeors and the all hydrometeor case a_{ILRS}. The labels in the legend correspond to the atmospheric composition suffix X. Note different values on the abcissa in the different plots.

For the LWC Jacobians (Fig. 8, top row), the lines group in two sets in both channels. In the 89.0 GHz channel, the signal is reduced in the presence of RWC in the lower levels. The presence of frozen hydrometeors does not alter the signal much. The pairs not including RWC, a_{IL} and a_{LS}, almost give the same Jacobian as a_L, while both ~~,~~a_{LR} and the all-hydrometeors case a_{ILRS} have a smaller peak and are very close up to about 700 hPa. Above that level, SWC has a greater influence. The Jacobian for a_{LS} deviates from the one of a_L and the all-hydrometeor case a_{ILRS} approaches the curve for the case a_{LS}. The change of behaviour near 700 hPa is due to the height ranges where SWC ~~, or RWC respectively, occur. Near this height~~or RWC occur, respectively. Near 700 hPa, the melting layer of the idealised atmosphere is located (see Fig. 3).

The 243.2 GHz channel has its largest sensitivity for the detection of RWC higher up in the atmosphere than the channel at 89 GHz and therefore does not exhibit such a transition. The two cases a_L and a_{LR} which only contain liquid hydrometeors have negative LWC Jacobians, while the presence of any frozen hydrometeors results in positive LWC Jacobians. The largest

signal comes from the all-hydrometeors case a_{ILRS}, the smallest positive one from the combination of LWC with IWC, i.e. a_{IL}.

This again can be understood if we think of the other cloud hydrometeors as contributors to the mixture of signals from all heights and hydrometeors, which result in the respective brightness temperature. The paths of the other cloud hydrometeor types, the surface and the H2O create a radiative background for the hydrometeor type in question. At 89.0 GHz, the presence of RWC already increases the brightness temperature, therefore the emission from LWC only adds a smaller positive increment compared to an atmosphere where only LWC is present. At 243.2 GHz, the scattering by frozen particles decreases the measured brightness temperature such that the emission by LWC adds a positive increment instead of a negative one if no IWC or SWC is present. These effects are not linear and can not just be added up.

For RWC (Fig. 8, bottom row), in the 89.0 GHz channel we also find a grouping of the Jacobians similar ~~as for~~ to LWC. For RWC the sign of the signal depends on the height. The lower levels cause a warmer background, such that the higher levels' contribution is negative compared to it. In the 243.2 GHz channel, the signal from rain is negative with the exception of a small positive contribution near the ground. The addition of any of the other hydrometeor types decreases the amplitude of the Jacobian. Each hydrometeor type alone, LWC, IWC and SWC, gives a cooling signal and therefore causes a colder background in the mixture compared to the case where only RWC is present.

Figure 9 shows the corresponding figures for the frozen hydrometeors IWC and SWC for the two channels. Since ~~here~~ the main interaction of the frozen particles with the radiation is scattering, the signal is robustly negative. In the 89.0 GHz channel, the IWC Jacobians for a_I and a_{IS} as well as the SWC Jacobians for a_S and a_{IS} are very ~~close~~similar. IWC and SWC only ~~little~~ marginally influence each other in that channel. The addition of liquid hydrometeors below the frozen ones leads to a stronger signal for IWC and SWC, because the liquid hydrometeors provide a warmer background for the frozen hydrometeors. In the 243.2 GHz channel, the picture is almost the same. In this channel, however, the signals from the frozen hydrometeors are much stronger, and the combination of IWC and SWC results in a considerably stronger cooling signal for both cloud hydrometeor types. Therefore the Jacobians for the all-hydrometeors case a_{ILRS} lie between a_{IS} and the other shown cases.

6.3 Information content

The ~~question is how much the information we gain~~ amount of the information gained from the observation depends on the composition of the atmosphere. Fig. 10 and Table 4 summarise ΔDOF for the 16 different atmospheric compositions, observed with the full set of channels and observed with the ICI channels. ~~We did not show the~~ The analysis for particle mean mass ($\bar{m}$~~Jacobians~~) Jacobians was not shown in the previous sections, but we include the values for their information content in this section to show the potential of new sensors ~~in this frequency range with regard to observing~~ observing at frequencies of 183 GHz and higher to observe microphysical properties of the particles.

~~For the~~ The main focus is on the detection of frozen hydrometeors, but in the following also the information content for liquid hydrometeors is included in the discussion. Liquid water retrievals at lower microwave channels are an established technique. For example a higher number of frequencies within the sounding regions between 50 and 57 GHz, which could be used in combination with the 118.75 GHz channels would be able to retrieve liquid cloud and precipitation, as was shown by

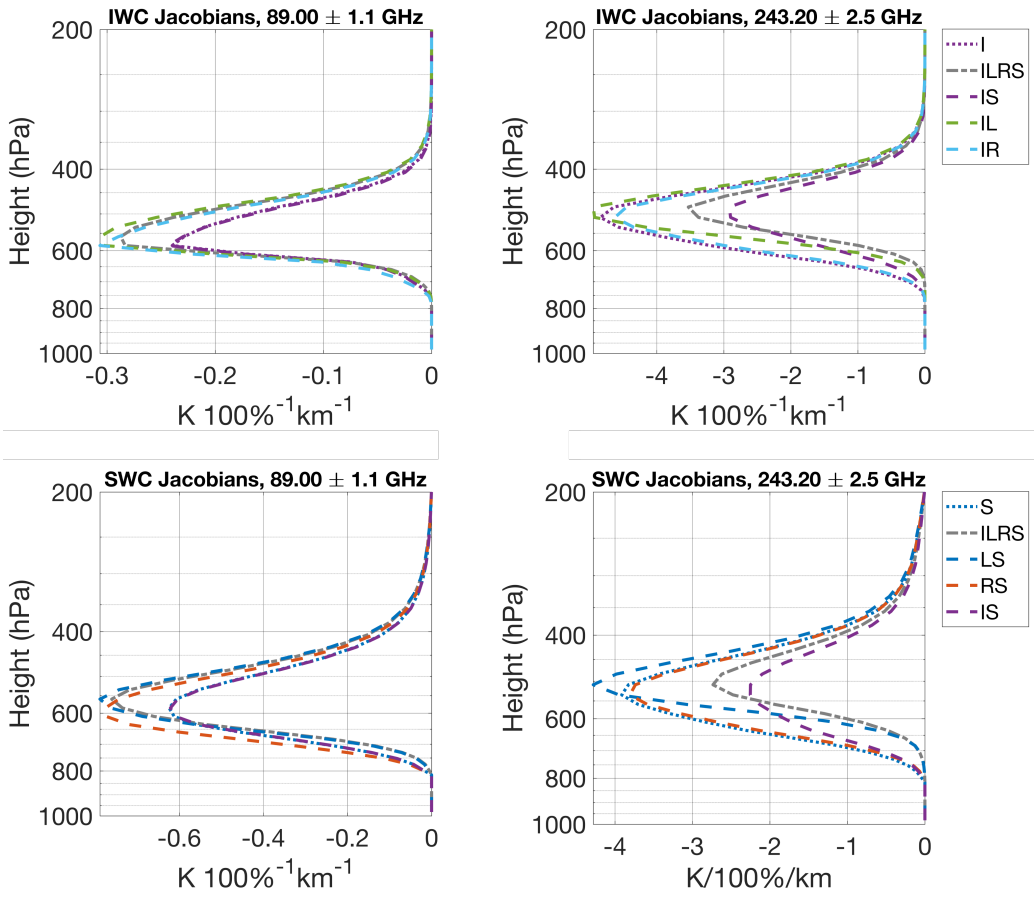

Figure 9. Same as Fig. 8, but for IWC (top row) and SWC (bottom row).

Bauer and Mugnai (2003). We lack channels in the region between 50 and 57 GHz, therefore in this analysis, we do not expect to have a great ability to detect liquid hydrometeors. We set our main focus on frozen hydrometeors. Nevertheless they will be discussed along with the information content on frozen hydrometeors and be treated as a side parameter for the detection of the frozen hydrometeors.

For the full set of channels, the total information content reaches up to values as high as ~~15.42~~ 12.15 for a_{ILRS} and is lowest for the clear sky case a_V with ~~3.55~~ 3.44 (Table 4).

Naturally, the more complex the atmosphere is, the higher ~~is~~ the overall possible total information content ~~since the~~ is. The initial degrees of freedom for these cases are more numerous and a greater portion of the channels can be used to reduce them (Fig. 10). ~~Also, it is very clear that once frozen hydrometeorsare present in the atmosphere the information content considerably increases by more than 3 compared to atmospheres which only contain liquid hydrometeors, because the Jacobians for frozen atmospheres have larger values and also much more channels are sensitive to these hydrometeor types (see Figs. 6 and 7). The presence of frozen hydrometeors slightly reduces the information about liquid ones. Also~~ The major part of the information

Table 4. Information content ΔDOF. Shown are mean of the total ΔDOF over the 16 different compositions, minimum and maximum of the total ΔDOF, and ~~of~~ the ~~the~~ mean, minimum and maximum ΔDOFs for hydrometeor mass densities and the corresponding particle mean masses ($\bar{m}$)~~found in~~ . The results refer to the set of 16 atmospheric combinations~~for~~ , used were all channels and ~~for~~ the ~~ICI like~~ reduced set of channels for ICI.

	all channels min | **mean** | max	ICI channels min | **mean** | max
total	~~3.55~~ 3.44 | ~~**11.23**~~**9.14** | ~~15.42~~ 12.15	~~2.73~~ 2.65 | ~~**7.60**~~**6.19** | ~~9.99~~ 8.20
H2O	~~0.66~~ 1.21 | ~~**1.68**~~**1.96** | ~~3.55~~ 3.44	~~0.50~~ 0.92 | ~~**1.14**~~**1.40** | ~~2.73~~ 2.65
~~LWC~~ IWC	~~2.05~~ 2.58 | ~~**2.36**~~**3.10** | ~~2.93~~ 3.65	~~0.69~~ 2.29 | ~~**0.94**~~**2.76** | ~~1.62~~ 3.32
~~IWC~~ SWC	~~4.28~~ 1.58 | ~~**4.99**~~**2.57** | ~~5.63~~ 3.56	~~3.80~~ 1.23 | ~~**4.50**~~**2.27** | ~~5.43~~ 3.44
~~RWC~~ IWC $\bar{m}$	~~1.14~~ 2.78 | ~~**1.81**~~**3.28** | ~~2.94~~ 3.88	~~0.02~~ 2.28 | ~~**0.27**~~**2.70** | ~~1.41~~ 3.20
SWC $\bar{m}$	~~3.89~~ 1.17 | ~~**4.84**~~**1.73** | ~~5.75~~ 2.42	~~3.16~~ 0.87 | ~~**4.25**~~**1.31** | ~~5.49~~ 1.77
LWC ~~$\bar{m}$~~	~~0.11e-3~~ 1.41 | ~~**0.35e-3**~~**1.69** | ~~1.02e-3~~ 2.20	~~1.1e-4~~ 0.16 | ~~**3.5e-4**~~**0.42** | ~~0.1e-4~~1.00
~~IWC $\bar{m}$~~ RWC	~~1.25~~ 0.72 | ~~**2.38**~~**1.08** | ~~3.49~~ 1.89	~~0.69~~ $1.8{\cdot}10^{-3}$ | ~~**1.51**~~**0.13** | ~~2.44~~0.94
~~RWC~~ LWC $\bar{m}$	~~0.74~~ $0.5{\cdot}10^{-3}$ | ~~**1.01**~~**0.8**$\cdot10^{-3}$ | ~~1.39~~ $1.3{\cdot}10^{-3}$	~~1.0e-4~~ $0.1{\cdot}10^{-3}$ | ~~**6.8e-2**~~**1.8**$\cdot10^{-3}$ | ~~0.378~~$2{\cdot}10^{-3}$
~~SWC~~ RWC $\bar{m}$	~~1.28~~ 0.62 | ~~**1.79**~~**0.91** | ~~2.60~~ 1.30	~~0.96~~ $0.1{\cdot}10^{-3}$ | ~~**1.40**~~**0.5**$\cdot10^{-3}$ | ~~1.92~~$1.6{\cdot}10^{-3}$

comes from the frozen hydrometeors. IWC gains most information for both the mass density (3.10 on average) and the particle mean masses (3.28 on average). The information content for the mean mass of IWC is greater than the one for the mass density of IWC. It is necessary to keep in mind the specific choice of the a priori assumptions. The information content is in principle high for IWC. The proportion between the information content for the mass density and the mean mass of IWC may depend on the choice of the thresholds for the mass density and the mean mass used to calculate the error covariance in ln-space (see Sect. 4.2 and discussion at the end of this section).

SWC gains an information content of 2.57 on average. The mean mass of snow gains 1.73 on average. IWC and SWC compete for the information. If both are included, both their information contents ~~slightly decrease~~by less than 1. decrease. The decrease is stronger for SWC in the presence of IWC than for IWC in the presence of SWC. This mirrors the behaviour of the Jacobians discussed above. If both frozen hydrometeor types are present, the absolute values of the Jacobians decrease. The ~~overall picture is the same for both, land and ocean, with only slight changes in the ranking of the total information content (not shown). For the higher land emissivities, the cases a_{ILRS}, a_{IL} and a_{LR} are shifted one position down each in that case, which means that a_{IRS}, a_{RS} and a_R are shifted one position up each. However, the respective pairs have very similar values in both cases and small changes in the information content easily lead to a slightly different ranking of the atmospheres.~~

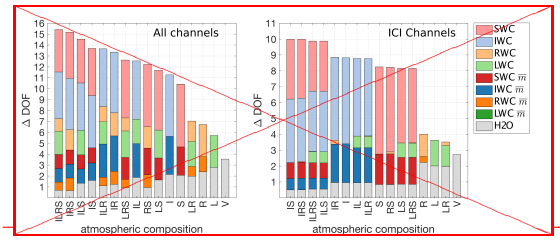

~~Information content ΔDOF for all atmospheres, ranked after the total ΔDOF. Results for the full set of channels are shown on the left, results for channels corresponding to ICI are shown on the right. Both were calculated with $\epsilon = 0.6$.~~

~~IWC and SWC give on average the highest ΔDOF of 4.99 and 4.84 (see Table 4). The spread~~ spread of the information content for the different atmospheric compositions is slightly higher for SWC, but the minimum information content is high for both, ~~4.28~~ 2.58 for IWC and ~~3.89~~ 1.58 for SWC. The ~~mean information content of 2.36 for LWC is much lower, and we get least mean information about RWC (1.81). The finding for LWC is in agreement with the study by ?, who found that with a limited set of channels in the window regions at 31, 90 and 150~~outer channels of the 118 ~~GHz the information content yields up to 2 pieces of information and a profile retrieval for LWC is not possible. Our channels larger than~~ GHz line, the window channels below, and the channel at 157 GHz ~~do not add much more information because the channels are only little sensitive to LWC (see Fig. 6)~~ add a considerable amount of information for LWC (1.69 on average) and some for RWC (1.08). For H2O under clear sky conditions, ~~we gain~~ a maximum ΔDOF of ~~3.55~~3.44 is gained, which decreases in the presence of clouds. Once hydrometeors are present in the atmospheric column, the information content for H2O is considerably reduced down to ~~0.66~~ 1.21 for the case ~~a_{TRS}. For clear sky, with~~ a_{ILRS}.

The overall picture is the same for both land and ocean, with only slight changes in the ranking of the ~~large set of channels we expected better sounding capacities of the sensor (i.e., a larger~~ total information content according to the total Δ~~DOF). The comparably low values we get are likely due to the high a priori autocorrelation of H2O which is inherent in the model (cp. Fig. 2).~~

~~For IWC and SWC we also find some considerable information about the particle mean masses. The mean information over all cases is even higher than the mean information for H2O alone. Therefore with the chosen channels it is also possible to some extent to gain information about ice microphysics. For the liquid hydrometeors, this is hardly possible, and~~ DOF (not shown). For the ~~mean information content for RWC is smaller than one. Especially for LWC the values are almost zero~~higher land emissivities, the cases a_{ILRS}, a_{IRS} are swapped. However, their information contents have very similar values in both cases and a small change in the information content easily leads to a slightly different ranking of the atmospheres.

~~We now set our focus on ICI and reduce the~~

Now the focus is set on ICI, which is designed to detect frozen hydrometeors. The set of channels ~~to the 11~~ is reduced to the eleven channels which correspond to this instrument (see Table 2). Naturally, the resulting total mean ΔDOF of ~~7.60~~ 6.19 is smaller than before because the number of channels is smaller~~, but this~~. This reduction is mostly at the cost of information about the liquid hydrometeors, not the frozen hydrometeors~~. For the liquid hydrometeors, on average we only get 0.94 for LWC and 0.27 for RWC~~, because the channels below 183 GHz are missing entirely in this case. For IWC the mean information

content is only slightly reduced to ~~4.50~~2.76, and for SWC to ~~4.25~~2.27. For the particle mean masses, ~~the one for IWCis considerably reduced to 1.51~~ ΔDOF for IWC $\bar{m}$ is reduced to 2.70 and the one for SWC $\bar{m}$ is slightly reduced to ~~1.40~~ 1.31 (Tab 4). ~~This finding suggests that the channels below 183 GHz, which are sensitive to IWC (cp. Fig. 7), add a considerable amount to the information about the IWC mean particle mass~~The information content for liquid hydrometeors is considerably reduced to 0.42 for LWC and to 0.13 for RWC.

In the ranking according to the total ΔDOF (Fig. 10) the atmospheres nicely ~~group into four~~ separate into three groups. The ~~ones containing IWC and SWC~~ atmospheres containing IWC build the group with highest total ΔDOF, ~~the ones~~ those containing SWC but no IWC rank second~~, closely followed by the ones containing IWC but no SWC~~. As before, the four atmospheres with the least information content are ~~the ones not containing~~ those without any frozen hydrometeors. ~~We also gain~~ Also information about the microphysical properties of the frozen ~~particles, although the one for IWC is considerably~~ hydrometeors is gained, although it is reduced compared to the full set of channels. ~~The results are in agreement with previous sections, since we already found that for liquid particles the information mainly stems from the channels lower than 183 GHz and for the frozen ones from the higher channels.~~ For the purpose of ICI it is no disadvantage to leave out the lower channels. ICI's focus is on the detection of cloud ice, and its ability to observe it on the global scale with a large spatial coverage seems to be unprecedentedly high.

We are aware that the results discussed in this section depend on the definition of the a priori covariance error. They especially depend on the choice of the lower threshold for the calculation of the covariance in ln space. If a very large threshold is assumed, the information content will be significantly diminished because there is only little variance left. For a very small numerical threshold, the variance will be large, and we will gain too much information. The dependence of the mean information content on the chosen threshold is shown in Fig. 11 for all hydrometeors for both mass density and mean mass. For cloud ice and snow,

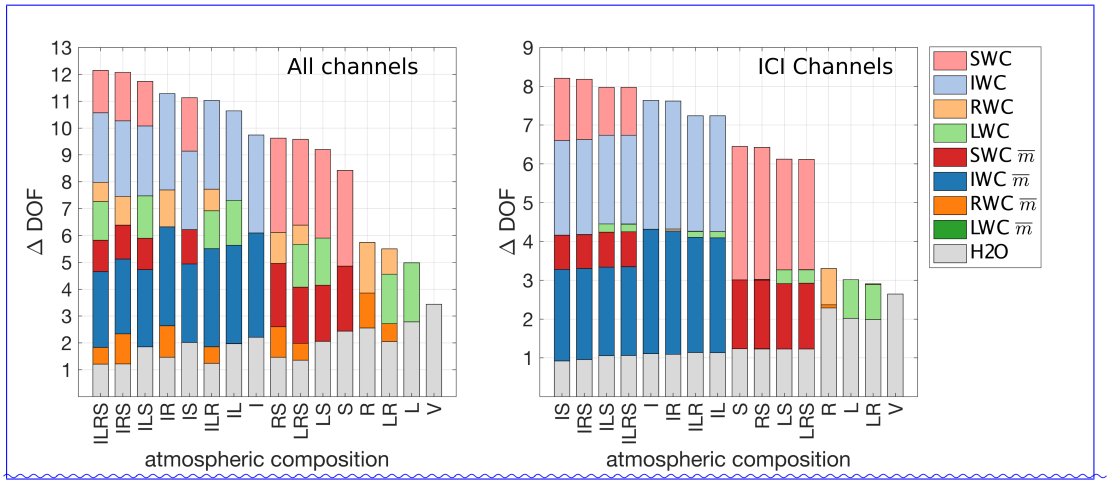

Figure 10. Information content ΔDOF for all atmospheres, ranked according to the total ΔDOF. Results for the full set of channels are shown on the left, results for channels corresponding to ICI are shown on the right. Both were calculated with $\epsilon = 0.6$.

also the range between minimum and maximum ΔDOF is shown. The mean information content for IWC and SWC decreases from 4.7 down to about 1.5 for thresholds from 10^{-16} kg m^{-3} up to 10^{-5} kg m^{-3}. The mean information content for IWC $\bar{m}$ and SWC $\bar{m}$ increases by 1.6 or 0.6, respectively. The dependence of the mean information contents for the liquid hydrometeor mass density and mean masses is weaker. The spread of the minimum and maximum for SWC shows little dependence on the threshold for the mass densities. For IWC, the spread decreases for the mass density but increases for the mean masses. The threshold is only varied for the mass densities, but not for the mean masses. The dependence of the information content for the mean masses is due to the fact that a combined analysis of all variables is performed. Furthermore, the cross correlations between mass densities and mean mass will cause a change of the information content of the mean masses.

For this analysis, thresholds were chosen, which are as physically based as possible (see Sect. 4.2). In particular, we use 10^{-7} kg kg^{-1} for the mass densities. Since this study is based on a spring time case from the mid-latitudes, the variance is likely smaller than one would expect if a whole year was taken into account.

6.4 Realistic atmospheric profiles

So far ~~we have only analysed~~ only one single, smooth idealised cloudy profile was analysed. To consolidate the results from the previous section, we have randomly drawn 90 more realistic cloudy profiles directly from the 10 000 ICON profiles, which were used to create the mean profile (see Sect. 5.2). ~~We calculate the~~ The information content ΔDOF was calculated in the same way as before. Although an even greater dataset would be desirable, the calculation of the Jacobians with ARTS is numerically rather expensive and we had to trade extensive statistics against computing time.

Figure 12 gives an overview of the information contents for the different hydrometeor types depending on the respective hydrometeor paths in the atmospheric column. The results from the idealised atmosphere presented above are substantiated in this statistical approach. Naturally the system tends to higher information contents for higher mass contents of the respective

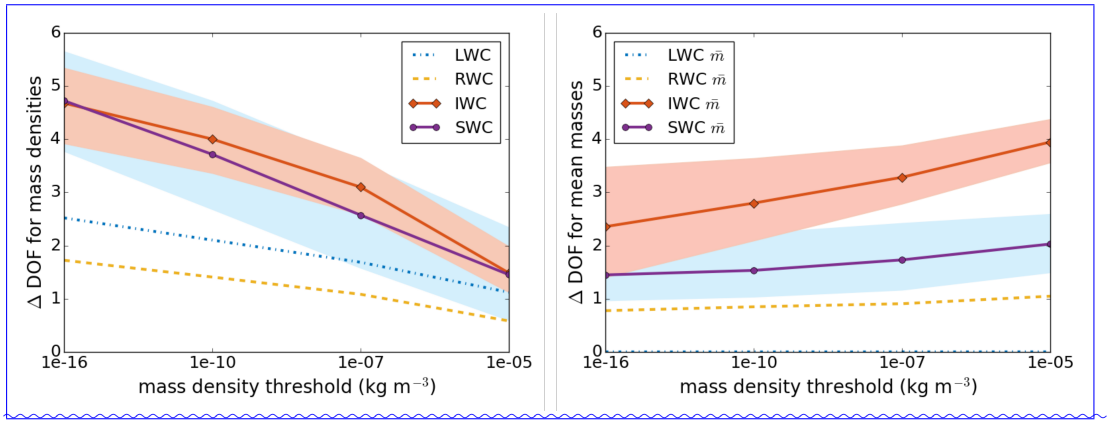

Figure 11. Dependence of information content on the thresholds for the mass density in the calcultion of the a priori covariance error (see Sect. 6.3 for details).The lines show the mean information content over the 16 atmospheres, the shaded areas mark the spread between the minimum and maximum information content over the atmospheres for cloud ice (red) and snow (blue).

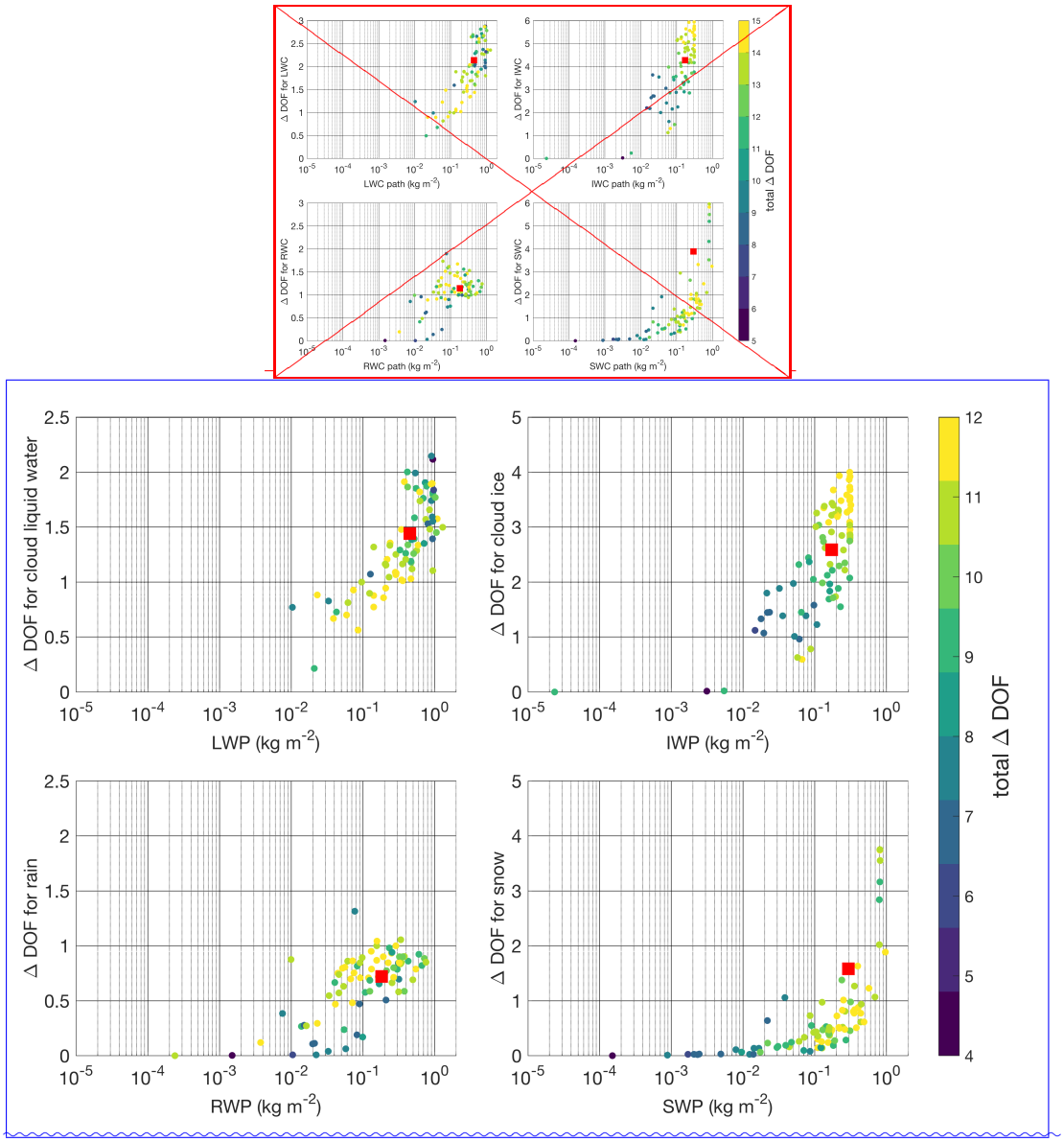

Figure 12. ΔDOF for the different hydrometeor mass densities over their respective column integrated path for 90 realistic atmospheres and the idealised atmosphere. The total ΔDOF is illustrated by color. The red square corresponds to the value from the idealised base profile. Note the different y axis for liquid and frozen hydrometeors.

hydrometeor. The values are in a similar range as ~~we~~ they were found above, except for SWC. For SWC, the ΔDOF from the idealised atmosphere ~~is amongst the outliers~~ tends towards higher information contents than most of the realistic atmospheres, even though the path is well in the range of paths from ~~the~~ those 90 atmospheres. This may be due to the fact that we ~~took care to have~~ tried to include all hydrometeor types in ~~our idealised profile and that for~~ the idealised profiles. In most realistic

profiles ~~, the~~ combination of snow and liquid clouds ~~or rain is seldom~~is rare. Thus, in general we expect to gain slightly less information on SWC than ~~we~~ was found for the idealised mean atmosphere.

For ~~IWC and SWC~~ cloud ice and snow, high total ΔDOFs tend to ~~be at high paths~~occur for high integrated path values IWP and SWP. For the liquid hydrometeors, ~~the~~ a relationship between high paths and high total information content is not found. On the contrary, for LWC the low total ΔDOFs tend to be at the upper end of ~~the LWC paths~~LWP, where the cloud is mainly liquid and only little frozen water mass is present. If ice is present in the cloud, the liquid hydrometeors will be ~~quickly consumed~~ consumed quickly by the Bergeron-Findeisen process and riming, yielding lower ~~LWC paths~~ LWPs but higher total ΔDOFs. The ~~most comforting result from the statistical analysis are the~~ overall high information contents ~~we gain~~ gained for frozen hydrometeors ~~, which~~ again points to the ability of sensors with such high microwave channels to observe ice and snow particles in clouds on a global scale robustly regardless of the atmospheric composition.

Some caution has to be ~~payed~~ paid with regard to the physical assumptions underlying the scattering and absorption properties of ice particles. For example, Birman et al. (2017) found that changes in the size distribution and scattering properties can shift the information content from IWC to solid precipitation. Also, contrary to ~~our~~ this study, Brath et al. (2018) did not find their retrieval ~~being~~ was sensitive to IWC using the same channels. They base their analysis on ICON simulations with a one-moment scheme, where the size distributions for IWC and SWC are more distinct and hardly overlap, and where the IWC distribution is shifted to smaller ice particles (Sect. 3.1). Therefore the information content is distributed differently between IWC and SWC. In nature, this arbitrary distinction between IWC and SWC does not exist and we only gain information about the whole ~~bunch~~ set of frozen hydrometeors at once, only limited by the size and amount of the particles, and depending on their shape.

In summary, the analysis of the model atmospheres with their different compositions shows satisfactory results. Despite the strong interdependencies of the ~~cloudy Jacobians~~ Jacobians for cloudy conditions presented in Sect. 6.2 the information content about the frozen hydrometeors proved to be high, independent of the atmospheric composition. This is especially due to the channels at high frequencies, ~~which are only little sensitive to liquid water, and~~ for which the Jacobians peak at different heights. Satellite missions such as ICI on MetOp SG, which employ a set of these high frequency channels therefore have a great potential to provide a robust retrieval of cloud ice and snow. For these frozen hydrometeors, ~~contrary to the liquid ones,~~ even an estimation of a profile may be possible, because the channels give information about different heights in the atmosphere and we get ΔDOFs ~~of 4 to almost 5~~up to four for IWC, which corresponds to ~~4 to 5~~ four different heights. Also, especially for cloud ice, ~~we consistently gain~~ consistently some insight into the microphysical properties is gained, i.e., about the mean particle mass.

To observe liquid hydrometeors, ~~also lower channels such as the ones from MWI would be required. In principle we gain only little information on LWC and RWC, which is slightly dependent on the surface, which it is even decreased in the presence of cloud ice or snow. Profile retrievals for the liquid hydrometeors do not appear to be possible at all with neither setup.~~

~~Passive microwave instruments which employ channels higher than the well established 183.31~~the lower channels from Deimos and Mars proved to be useful. These channels in the regions between 50 and 57 GHz ~~gain more and more attention as a valuable tool to observe clouds on the global scale from space. The high frequencies especially serve to measure IWC and~~

SWC. In fact, the upcoming MetOp-SG mission will have ICI on board, which employs channels in the range from 183.31and around 118.75 GHz up to 664.0 GHzGHz are employed on MWI on Metop-SG. MWI uses, amongst others, channels in these regions to retrieve precipitation over land and sea (Bauer and Mugnai (2003)).

In the past, many studies focused on the existing and well-established instruments such as AMSU-B, which measures at 89, 150 and 183.31 GHz (e.g. Hong et al., 2005, and references therein). The studies focused on the influence of the surface and of single hydrometeors on the brightness temperature spectra. Also, several studies focused on the selection of the most suitable channel sets for such instruments (Di Michele and Bauer, 2006; Jiménez et al., 2007) and on the gain of information content for hydrometeors from hyperspectral sensors (Birman et al., 2017). In

7 Conclusions

In this study, we performed an all-sky information content analysis was performed for passive microwave instruments . Especially, we focused on the dependence of the information content for a certain cloud hydrometeor type on the atmospheric composition and analysed whether it is robust across the different compositions. This is worthwhile because the cloud Jacobians are highly interdependent. Also, some authors found that for example the signal of cloud ice in the 183.31 GHz channel is much weaker if the clouds precipitate compared to the signal of cloud ice from non-precipitating clouds (Greenwald and Christopher, 2002).

We chose the setups of MARSSusing channels from the instruments MARSS, Deimos and ISMAR, which have been flown in a recent flight campaign and complemented them by two low-frequency precipitation channels from Deimos. The resulting channels range from 23.8 GHz up to 874.4 GHz. We based our study on a high resolution simulation from the ICON model with a the study on an ICON simulation employing the two-moment microphysics scheme from Seifert and Beheng (2006). The information content was quantified by the reduction of the degrees of freedom basing on optimal estimation theory. The required Jacobians were calculated explicitly by Seifert and Beheng (2006) and calculated Jacobians with the radiative transfer simulator ARTS (Eriksson et al., 2011; Buehler et al., 2005)(Buehler et al., 2005, 2018; Eriksson et al., 2011).

An analysis of idealised profiles from ICON containing different combinations of LWC, IWC, RWC and SWC showed that the different Jacobians Jacobians for the hydrometeors and H2O have strong interdependencies. Each component of the cloud changes the radiative background for the others, such that its presence shields weakens or strengthens their contributions to the measured brightness temperature in the respective channel. The warming signal from H2O in the 89.0 and outermost 118.75 GHz channel is shielded weakened by liquid hydrometeors, and the negative signal in the channels higher than 183.31 GHz turns positive in the presence of frozen hydrometeors in the atmospheric column seen by the channel. The signals from LWC and RWC strongly depend on the presence of other hydrometeor types and even change sign in some channels depending on the composition of the atmosphere. The signal from frozen hydrometeors is always negative at all heights. It tends to get stronger in the presence of liquid hydrometeors, which is contrary to the findings of Greenwald and Christopher (2002) for 183.31 GHz. It slightly weakens for both The signal from frozen hydrometeors slightly weakens if both frozen hydrometeor types, IWC and SWC, are present at the same time.

Despite these interdependencies of the Jacobians, the information content is robust with regard to the composition of the atmosphere. ~~The information we gain about LWC is low and does not allow for profile or microphysical retrievals, which is in accordance with findings from ?.~~ Due to the higher channels beyond 183.31 GHz the information content on the frozen hydrometeors is high. On average ΔDOF reaches ~~4.99 and 4.84~~ 3.10 and 2.57 for IWC and SWC. This implies a potential to retrieve profiles of the frozen hydrometeors and is due to the Jacobians of the relevant channels peaking at different heights. Also, the use of these high ~~channels enables~~ frequency channels enables us to observe microphysical properties of IWC and SWC. Especially for IWC~~mean masses we find~~ $\bar{m}$ a high information content of ~~2.38, the one from SWCis slightly lower (1.79~~3.28 is found. The information content found for SWC $\bar{m}$ is lower (1.73). However, one has to keep in mind that the distinction between IWC and SWC in the atmospheric model is inherent in the microphysical parameterisation scheme and can not be made in reality, where the transition between the hydrometeors is continuous. Also, the model inherent microphysical size distributions influence the results. For example, the two-moment scheme used in this study tends to larger frozen hydrometeors and fewer small cloud ice particles than for example the one moment scheme from McFarquhar and Heymsfield (1997). As expected, the employed channels below 183 GHz observe mainly the liquid hydrometeors. With the full set of channels, an information content of 1.69 for LWC and of 1.08 for RWC is gained. There is only very little information about the mean mass of the two liquid hydrometeors. However, the focus of this study was on frozen hydrometeors and the channels were chosen accordingly. For a more decent retrieval of liquid water more channels in the lower regions would have to be employed as for example explained by Bauer and Mugnai (2003).

We have consolidated the results from the idealised profile with a set of 90 more realistic cloudy profiles from the ICON model. As expected ~~we find a~~ close relation between the hydrometeor path and the information we gain about that hydrometeor was found. The highest total information contents stem from atmospheres containing frozen hydrometeors, which is due to the fact that the scattering signal from IWC and SWC is strong, especially in the higher channels used in this study. ~~We have to add that within these 90 profiles we find that the information content on SWC for the idealised case is amongst the outliers towards higher information contents.~~

To explore the potential of ICI to observe cloud ice amount and microphysical properties on the global scale we also analysed the all-sky information content gained from that instrument. ~~We~~ It was found that the information with regard to IWC (~~4.50~~2.76) and SWC (~~4.25~~2.27) is only slightly lower than for the full channel set and that there is still information about the microphysical properties of the frozen particles, even though for IWC $\bar{m}$ mean masses it is considerably reduced to ~~1.51~~ 2.70 compared to the full channel value of ~~2.38~~3.28. The good performance of the ICI channel set for cloud ice and snow retrievals is very encouraging for the upcoming mission.

Acknowledgements. This work was funded by the European Space Agency (ESA) under the Contract Nr. 4000113023/13/NL/MV and by the Universität Hamburg's Cluster of Excellence "Integrated Climate System Analysis and Prediction" (CliSAP, funded by DFG). The authors thank the Max-Planck Institute for Meteorology, Hamburg, and the project HD(CP)^2 for providing the atmospheric model data for this study and the ARTS community for providing and developing the radiative transfer model ARTS. We thank Axel Seifert for his support with regard

to the two-moment microphysics scheme, Rémy Roca and Jean-Franǫis Mahfouf for the very valuable scientific discussions and support, and Oliver Lemke for technical support of the study.

Furthermore the authors would like to thank two anonymous reviewers for their very valuable comments and discussion, especially with regard to the a priori assumptions.

References

Accadia, C., Schlüssel, P., Phillips, P. L., and Wilson, J. J. W.: The EUMETSAT Polar System-Second Generation (EPS-SG) micro-wave and sub-millimetre wave imaging missions, in: SPIE Remote Sensing, vol. 8889, pp. 88 890H–88 890H, International Society for Optics and Photonics, doi:10.1117/12.2028676, 2013.

Aires, F., Prigent, C., Orlandi, E., Milz, M., Eriksson, P., Crewell, S., Lin, C.-C., and Kangas, V.: Microwave hyper-spectral measurements for temperature and humidity atmospheric profiling from satellite: the clear-sky case, J. Geophys. Res., 120, 11,334–11,351, doi:10.1002/2015JD023331, 2015.

Aires, F., Prigent, C., Buehler, S. A., and Eriksson, P.: Towards more realistic hypotheses for the information content analysis of cloudy/precipitating situations – Application to an hyper-spectral instrument in the microwaves, Q. J. R. Meteorol. Soc., in press.

Bauer, P. and Mugnai, A.: Precipitation profile retrievals using temperature-sounding microwave observations, J. Geophys. Res., 108, doi:10.1029/2003JD003572, 2003.

Bennartz, R. and Bauer, P.: Sensitivity of microwave radiances at 85–183 GHz to precipitating ice particles, Radio Sci., 38, doi:10.1029/2002RS002626, 2003.

Birman, C., Mahfouf, J.-F., Milz, M., Mendrok, J., Buehler, S. A., and Brath, M.: Information content on hydrometeors from millimeter and sub-millimeter wavelengths, Tellus, 69, doi:10.1080/16000870.2016.1271562, 2017.

Bonsignori, R.: The Microwave Humidity Sounder (MHS): in-orbit performance assessment, doi:10.1117/12.737986, http://dx.doi.org/10.1117/12.737986, 2007.

Boucher, O., Randall, D., Artaxo, P., Bretherton, C., Feingold, G., Forster, P., Kerminen, V.-M., Kondo, Y., Liao, H., Lohmann, U., Rasch, P., Satheesh, S., Sherwood, S., Stevens, B., and Zhang, X.: Clouds and Aerosols, book section 7, p. 571–658, Cambridge University Press, Cambridge, United Kingdom and New York, NY, USA, doi:10.1017/CBO9781107415324.016, www.climatechange2013.org, 2013.

Brath, M., Fox, S., Eriksson, P., Harlow, R. C., Burgdorf, M., and Buehler, S. A.: Retrieval of an Ice Water Path over the Ocean from ISMAR and MARSS millimeter/submillimeter brightness temperatures, Atmos. Meas. Tech. Discuss., doi:10.5194/amt-2017-167, ~~in review, 2017.~~ 2018.

Buehler, S. A., Eriksson, P., Kuhn, T., von Engeln, A., and Verdes, C.: ARTS, the atmospheric radiative transfer simulator, J. Quant. Spectrosc. Radiat. Transfer, 91, 65–93, doi:10.1016/j.jqsrt.2004.05.051, 2005.

Buehler, S. A., Jiménez, C., Evans, K. F., Eriksson, P., Rydberg, B., Heymsfield, A. J., Stubenrauch, C., Lohmann, U., Emde, C., John, V. O., Sreerekha, T. R., and Davis, C. P.: A concept for a satellite mission to measure cloud ice water path and ice particle size, Q. J. R. Meteorol. Soc., 133, 109–128, doi:10.1002/qj.143, 2007.

Buehler, S. A., Defer, E., Evans, F., Eliasson, S., Mendrok, J., Eriksson, P., Lee, C., Jimenéz, C., Prigent, C., Crewell, S., Kasai, Y., Bennartz, R., and Gasiewski, A. J.: Observing Ice Clouds in the Submillimeter Spectral Range: The CloudIce Mission Proposal for ESA's Earth Explorer 8, Atmos. Meas. Tech., 5, 1529–1549, doi:10.5194/amt-5-1529-2012, http://www.atmos-meas-tech.net/5/1529/2012/, 2012.

Buehler, S. A., Mendrok, J., Eriksson, P., Perrin, A., Larsson, R., and Lemke, O.: ARTS, the atmospheric radiative transfer simulator — version 2.2, the planetary toolbox edition, Geosci. Model Dev., 11, 1537–1556, doi:10.5194/gmd-11-1537-2018, 2018.

Burns, B., Wu, X., and Diak, G.: Effects of precipitation and cloud ice on brightness temperatures in AMSU moisture channels, IEEE Transactions on Geoscience and Remote Sensing, 35, 1429–1437, doi:10.1109/36.649797, 1997.

~~Crewell, S., Ebell, K., Lohnert, U., and Turner, D. D.: Can liquid water profiles be retrieved from passive microwave zenith observations, Geophys. Res. Lett., 36, L06803, , 2009.~~

Defer, E., Galligani, V. S., Prigent, C., and Jimenez, C.: First observations of polarized scattering over ice clouds at close-to-millimeter wavelengths (157 GHz) with MADRAS on board the Megha-Tropiques mission, J. Geophys. Res., 119, 12 301–12 316, doi:10.1002/2014JD022353, 2014.

Desbois, M., Roca, R., Eymard, L., Viltard, N., Viollier, M., Srinivasan, J., and Narayanan, S.: The Megha-Tropiques mission, Proc. of SPIE, 4899, 172–183, 2002.

Di Michele, S. and Bauer, P.: Passive microwave radiometer channel selection based on cloud and precipitation information content, Q. J. R. Meteorol. Soc., 132, 1299–1323, doi:10.1256/qj.05.164, 2006.

Dipankar, A., Stevens, B., Heinze, R., Moseley, C., Zängl, G., Giorgetta, M., and Brdar, S.: A Large Eddy Simulation version of ICON (ICOsahedral Nonhydrostatic): Model Description and Validation, J. Adv. Model. Earth Syst., 7, 963–986, doi:10.1002/2015MS000431, 2015.

Duruisseau, F., Chambon, P., Guedj, S., Guidard, V., Fourrié, N., Taillefer, F., Brousseau, P., Mahfouf, J.-F., and Roca, R.: Investigating the potential benefit to a mesoscale NWP model of a microwave sounder on board a geostationary satellite, Quarterly Journal of the Royal Meteorological Society, 143, 2104–2115, doi:10.1002/qj.3070, http://dx.doi.org/10.1002/qj.3070, 2017.

Emde, C., Buehler, S. A., Davis, C., Eriksson, P., Sreerekha, T. R., and Teichmann, C.: A Polarized Discrete Ordinate Scattering Model for Simulations of Limb and Nadir Longwave Measurements in 1D/3D Spherical Atmospheres, J. Geophys. Res., 109, D24207, doi:10.1029/2004JD005140, 2004.

Eriksson, P., Ekström, M., Rydberg, B., Wu, D. L., Austin, R. T., and Murtagh, D. P.: Comparison between early Odin-SMR, Aura MLS and CloudSat retrievals of cloud ice mass in the upper tropical troposhere, Atmos. Chem. Phys., 8, 1937–1948, doi:10.5194/acp-8-1937-2008, 2008.

Eriksson, P., Buehler, S. A., Davis, C. P., Emde, C., and Lemke, O.: ARTS, the atmospheric radiative transfer simulator, Version 2, J. Quant. Spectrosc. Radiat. Transfer, 112, 1551–1558, doi:10.1016/j.jqsrt.2011.03.001, 2011.

Eriksson, P., Jamali, M., Mendrok, J., and Buehler, S. A.: On the microwave optical properties of randomly oriented ice hydrometeors, Atmos. Meas. Tech., pp. 1913–1933, doi:10.5194/amt-8-1913-2015, 2015.

Fox, S., Lee, C., Moyna, B., Philipp, M., Rule, I., Rogers, S., King, R., Oldfield, M., Rea, S., Henry, M., Wang, H., and Harlow, R. C.: ISMAR: an airborne submillimetre radiometer, Atmos. Meas. Tech., 10, doi:10.5194/amt-10-477-2017, 2017.

Geer, A. J. and Baordo, F.: Improved scattering radiative transfer for frozen hydrometeors at microwave frequencies, Atmos. Meas. Tech., 7, 1839–1860, doi:10.5194/amt-7-1839-2014, 2014.

Geer, A., Baordo, F., Bormann, N., Chambon, P., English, S., Kazumori, M., Lawrence, H., Lean, P., Lonitz, K., and Lupu, C.: The growing impact of satellite observations sensitive to humidity, cloud and precipitation, Q. J. R. Meteorol. Soc., 143, 3189–3206, 2017.

Greenwald, T. J. and Christopher, S. A.: Effect of cold clouds on satellite measurements near 183 GHz, J. Geophys. Res., 107, D13, doi:10.1029/2000JD000258, 2002.

Guerbette, J., Mahfouf, J.-F., and Plu, M.: Towards the assimilation of all-sky microwave radiances from the SAPHIR humidity sounder in a limited area NWP model over tropical regions, Tellus, 68, doi:10.3402/tellusa.v68.28620, 2016.

Heinze, R., Dipankar, A., Henken, C. C., Moseley, C., Sourdeval, O., Troemel, S., Xie, X., Adamidis, P., Ament, F., Baars, H., Barthlott, C., Behrendt, A., Blahak, U., Bley, S., Brdar, S., Brueck, M., Crewell, S., Deneke, H., Di Girolamo, P., Evaristo, R., Fischer, J., Frank, C., Friederichs, P., Goecke, T., Gorges, K., Hande, L., Hanke, M., Hansen, A., Hege, H.-C., Hoose, C., Jahns, T., Kalthoff, N., Klocke, D., Kneifel, S., Knippertz, P., Kuhn, A., van Laar, T., Macke, A., Maurer, V., Mayer, B., Meyer, C. I., Muppa, S. K., Neggers, R. A. J., Orlandi, E., Pantillon, F., Pospichal, B., Roeber, N., Scheck, L., Seifert, A., Seifert, P., Senf, F., Siligam, P., Simmer, C., Steinke, S., Stevens, B.,

Wapler, K., Weniger, M., Wulfmeyer, V., Zaengl, G., Zhang, D., and Quaas, J.: Large-eddy simulations over Germany using ICON: a comprehensive evaluation, Q. J. R. Meteorol. Soc., 143, 69–100, doi:10.1002/qj.2947, 2017.

Hewison, T.: The design of Deimos: A microwave radiometer with channels at 23.8GHz and 50.3GHz for the UK met. Research flight C-130 aircraft, in: IGARSS '95 - 1995 International Geoscience and Remote Sensing Symposium, Vols 1-3: Quantitative Remote Sensing for Science and Applications, edited by T.I. Stein, pp. 2261–2263, IEEE, Geosci & Remote Sensing Soc; Union Radiosci Int, 1995 International Geoscience and Remote Sensing Symposium (IGARSS 95), Florence, Italy, Jul 10-14, 1995, 1995.

Heymsfield, A. J.: On measurements of small ice particles in clouds, Geophys. Res. Lett., 34, n/a–n/a, doi:10.1029/2007GL030951, http://dx.doi.org/10.1029/2007GL030951, l23812, 2007.

Hong, G., Heygster, G., Miao, J., and Kunzi, K.: Sensitivity of microwave brightness temperatures to hydrometeors in tropical deep convective cloud system at 89-190 GHz channels measurements, Radio Sci., 40, RS4003, doi:10.1029/2004RS003129, 2005.

Hong, G., Yang, P., Baum, B. A., Heymsfield, A. J., Weng, F., Liu, Q., Heygster, G., and Buehler, S. A.: Scattering Database in the Millimeter and Submillimeter Wave Range of 100–1000 GHz for Nonspherical Ice Particles, J. Geophys. Res., 114, D06201, doi:10.1029/2008JD010451, 2009.

Jiménez, C., Buehler, S. A., Rydberg, B., Eriksson, P., and Evans, K. F.: Performance simulations for a submillimetre wave cloud ice satellite instrument, Q. J. R. Meteorol. Soc., 133, 129–149, doi:10.1002/qj.134, 2007.

Karouche, N., Goldstein, C., Rosak, A., Malassingne, C., and Raju, G.: MEGHA-TROPIQUES atellite mission: In Flight Performances Results, in: 2012 IEEE International Geoscience and Remote Sensing Symposium (IGARSS), IEEE International Symposium on Geoscience and Remote Sensing IGARSS, pp. 4684–4687, IEEE; IEEE Geosci & Remote Sensing Soc; DLR; ESA, doi:10.1109/IGARSS.2012.6350420, IEEE International Geoscience and Remote Sensing Symposium (IGARSS), Munich, GERMANY, JUL 22-27, 2012, 2012.

Liu, G.: A Database of Microwave Single-Scattering Properties for Nonspherical Ice Particles, Bull. Amer. Met. Soc., 89, 1563–1570, doi:10.1175/2008BAMS2486.1, 2008.

Macke, A., Seifert, P., Baars, H., Barthlott, C., Beekmans, C., Behrendt, A., Bohn, B., Brueck, M., Buehl, J., Crewell, S., Damian, T., Deneke, H., Duesing, S., Foth, A., Di Girolamo, P., Hammann, E., Heinze, R., Hirsikko, A., Kalisch, J., Kalthoff, N., Kinne, S., Kohler, M., Loehnert, U., Madhavan, B. L., Maurer, V., Muppa, S. K., Schween, J., Serikov, I., Siebert, H., Simmer, C., Spaeth, F., Steinke, S., Traeumner, K., Troemel, S., Wehner, B., Wieser, A., Wulfmeyer, V., and Xie, X.: The HD(CP)(2) Observational Prototype Experiment (HOPE) - an overview, Atmos. Chem. Phys., 17, 4887–4914, doi:10.5194/acp-17-4887-2017, 2017a.

Macke, A., Seifert, P., Baars, H., Barthlott, C., Beekmans, C., Behrendt, A., Bohn, B., Brueck, M., Buehl, J., Crewell, S., Damian, T., Deneke, H., Duesing, S., Foth, A., Di Girolamo, P., Hammann, E., Heinze, R., Hirsikko, A., Kalisch, J., Kalthoff, N., Kinne, S., Kohler, M., Loehnert, U., Madhavan, B. L., Maurer, V., Muppa, S. K., Schween, J., Serikov, I., Siebert, H., Simmer, C., Spaeth, F., Steinke, S., Traeumner, K., Troemel, S., Wehner, B., Wieser, A., Wulfmeyer, V., and Xie, X.: The HD(CP)(2) Observational Prototype Experiment (HOPE) - an overview, ATMOSPHERIC CHEMISTRY AND PHYSICS, 17, 4887–4914, doi:10.5194/acp-17-4887-2017, 2017b.

Mahfouf, J.-F., Birman, C., Aires, F., Prigent, C., Orlandi, E., and Milz, M.: Information content on temperature and water vapour from a hyper-spectral microwave sensor, Q. J. R. Meteorol. Soc., 141, 3268–3284, doi:10.1002/qj.2608, 2015.

Mätzler, C.: MATLAB functions for Mie scattering and absorption, version 2, IAP Res. Rep, 8, 2002.

Mätzler, C.: Thermal Microwave Radiation: Application for Remote Sensing, vol. 52 of *IET Electromagn. Waves Ser.*, chap. Microwave dielectric properties of ice, pp. 455–462, Inst. Eng. Technol., Stevenage, U. K., 2006.

McFarquhar, G. M. and Heymsfield, A. J.: Parameterization of Tropical Cirrus Ice Crystal Size Distribution and Implications for Radiative Transfer: Results from CEPEX, J. Atmos. Sci., 54, 2187–2200, doi:10.1175/1520-0469(1997)054<2187:POTCIC>2.0.CO;2, 1997.

McGrath, A. and Hewison, T.: Measuring the Accuracy of MARSS- An Airborne Microwave Radiometer, J. Atmos. Oceanic Technol., 18, 2003–2012, 2001.

Mlawer, E. J., Payne, V. H., Moncet, J.-L., Delamere, J. S., Alvarado1, M. J., and Tobin, D. C.: Development and recent evaluation of the MT_CKD model of continuum absorption, Phil. Trans. R. Soc. A, 370, 2520–2556, doi:10.1098/rsta.2011.0295, 2012.

Muller, B. M., Fuelberg, H. E., and Xiang, X.: Simulations of the Effects of Water Vapor, Cloud Liquid Water, and Ice on AMSU Moisture Channel Brightness Temperatures, J. Appl. Meteorol., 33, 1133–1154, 1994.

Pica, G., Alberti, G., Memoli, A., Santovito, M. R., Varchetta, S., Buralli, B., D'Addio, S., and Kangas, V.: MetOp Second Generation: A joint ESA/EUMETSAT mission for weather forecast and climate monitoring with an imaging radiometer, in: Proceedings of the 63rd International Astronautical Congress 2012 (IAC 2012), pp. 3132–3136, International Astronautical Federation (IAF), paper: IAC-12-B1.3.10, 2012.

Rodgers, C. D., ed.: Inverse Methods for Atmospheric Sounding: Theory and Practice, World Scientific Publishing, ISBN-10 981022740X, 2000.

Rothman, L. S., Gordon, I. E., Babikov, Y., Barbe, A., Benner, D. C., Bernath, P. F., Birk, M., Bizzocchi, L., Boudon, V., Brown, L. R., Campargue, A., Chance, K., Cohen, E. A., Coudert, L. H., Devi, V. M., Drouin, B. J., Fayt, A., Flaud, J.-M., Gamache, R. R., Harrison, J. J., Hartmann, J.-M., Hill, C., Hodges, J. T., Jacquemart, D., Jolly, A., Lamouroux, J., Le Roy, R. J., Li, G., Long, D. A., Lyulin, O. M., Mackie, C. J., Massie, S. T., Mikhailenko, S., Müller, H. S. P., Naumenko, O. V., Nikitin, A. V., Orphal, J., Perevalov, V., Perrin, A., Polovtseva, E. R., Richard, C., Smith, M. A. H., Starikova, E., Sung, K., Tashkun, S., Tennyson, J., Toon, G. C., Tyuterev, V. G., and Wagner, G.: The HITRAN2012 molecular spectroscopic database, J. Quant. Spectrosc. Radiat. Transfer, 130, 4–50, doi:10.1016/j.jqsrt.2013.07.002, 2013.

Seifert, A. and Beheng, K. D.: A two-moment cloud microphysics parameterization for mixed-phase clouds. Part 1: Model description, Met. Atm. Phys., 92, 45–66, doi:10.1007/s00703-005-0112-4, 2006.

Sreerekha, T. R., Buehler, S. A., O'Keeffe, U., Doherty, A., Emde, C., and John, V. O.: A strong ice cloud event as seen by a microwave satellite sensor: Simulations and Observations, J. Quant. Spectrosc. Radiat. Transfer, 109, 1705–1718, doi:10.1016/j.jqsrt.2007.12.023, 2008.

Stamnas, E., Lammert, A., Winkelmann, V., and Lang, U.: The HD(CP)2 Data Archive for Atmospheric Measurement Data, ISPRS International Journal of Geo-Information, 5, 124, doi:10.3390/ijgi5070124, http://www.mdpi.com/2220-9964/5/7/124, 2016.

Wan, H., Giorgetta, M. A., Zängl, G., Restelli, M., Majewski, D., Bonaventura, L., Fröhlich, K., Reinert, D., Rıpodas, P., Kornblueh, L., and Förstner, J.: The ICON-1.2 hydrostatic atmospheric dynamical core on triangular grids, Part I: formulation and performance of the baseline version, Geosci. Model Dev., 6, 735–763, doi:doi:10.5194/gmd-6-735-2013, 2013.

Warren, S.: Optical Constants of Ice from the Ultraviolet to the Microwave, Appl. Opt., 23, 1206–1225, doi:10.1364/AO.23.001206, 1984.

Weng, F., Zhao, L., Ferraro, R. R., Poe, G., Li, X., and Grody, N. C.: Advanced microwave sounding unit cloud and precipitation algorithms, Radio Sci., 38, 8068, doi:10.1029/2002RS002679, 2003.

Zhao, L. and Weng, F.: Retrieval of Ice Cloud Parameters Using the Advanced Microwave Sounding Unit, J. Appl. Meteorol., 41, 384–395, 2002.